Hypothalamic dopamine signalling regulates brown fat thermogenesis

Cintia Folgueira[1,2,3], Daniel Beiroa[2,3], Begoña Porteiro[2,3], Manon Duquenne[4], Emma Puighermanal[5], Marcos F. Fondevila[2,3], Silvia Barja-Fernández[1,3], Rosalia Gallego[6], René Hernández-Bautista[2], Cecilia Castelao[1,3], Ana Senra[2], Patricia Seoane-Collazo[2,3], Noemi Gómez-Lado[7,8,9], Pablo Aguiar[7,8,9], Diana Guallar[2], Miguel Fidalgo[2], Amparo Romero-Pico[2,3], Roger Adan[10], Clemence Blouet[11], Jose Luís Labandeira-García[2,12], Françoise Jeanrenaud[13], Imre Kallo[14], Zsolt Liposits[14], Javier Salvador[3,15], Vincent Prevot[4], Carlos Dieguez[2,3], Miguel López[2,3], Emmanuel Valjent[5], Gema Frühbeck[3,15], Luisa M. Seoane[1,3]* and Ruben Nogueiras[2,3]*

Dopamine signalling is a crucial part of the brain reward system and can affect feeding behaviour. Dopamine receptors are also expressed in the hypothalamus, which is known to control energy metabolism in peripheral tissues. Here we show that pharmacological or chemogenetic stimulation of dopamine receptor 2 (D2R) expressing cells in the lateral hypothalamic area (LHA) and the zona incerta (ZI) decreases body weight and stimulates brown fat activity in rodents in a feeding-independent manner. LHA/ZI D2R stimulation requires an intact sympathetic nervous system and orexin system to exert its action and involves inhibition of PI3K in the LHA/ZI. We further demonstrate that, as early as 3 months after the onset of treatment, patients treated with the D2R agonist cabergoline experience an increase in energy expenditure that persists for one year, leading to total body weight and fat loss through a prolactin-independent mechanism. Our results may provide a mechanistic explanation for how clinically used D2R agonists act in the central nervous system to regulate energy balance.

Obesity has reached epidemic prevalence, and much research has focused on homeostatic and hedonic mechanisms underlying overconsumption of food and the regulation of body weight. Dopamine has the ability to modulate food consumption by both reward (hedonic) and hypothalamic (homeostatic) pathways[1]. Among the five dopamine receptors (D1R, D2R, D3R, D4R and D5R), dopamine signalling through D1R[2–4] and D2R regulates food intake[1,5–7]. The increase in central dopaminergic signalling is often associated with the stimulation of feeding, while its decrease has the opposite effect; however, in the hypothalamus, the effects on food intake depend on the hypothalamic area targeted[8].

The clinical relevance of the D2R is well characterized and D2R agonists such as bromocriptine and cabergoline, have been widely used for the treatment of prolactinomas. Since 2009, bromocriptine has also been approved in the United States as an adjunctive treatment for type 2 diabetes[9], as it improves glucose tolerance and reduces fasting and postprandial plasma glucose levels in patients with diabetes[10–12]. In terms of energy homeostasis, obese humans have reduced dopamine levels and/or function[13]. Antipsychotic drugs that block D2R are associated with increased appetite, weight gain and development of diabetes[14,15] and morbidly obese humans have less D2R availability[8]. In addition, human studies have shown a higher prevalence of the *Taq1A* allele for the D2R in obese individuals[16] and genetic variants influencing D2R signalling affect a significant portion of the population[17]. However, the effects of bromocriptine and cabergoline on body weight are contradictory in different studies, albeit most of them non-randomized, reporting either a reduction or no significant effects on body weight[10,18] or no significant effects on body weight in obese patients or those with type 2 diabetes[19].

In this study, we found that the central stimulation of D2R increases brown adipose tissue (BAT) activity in lean and DIO rodents in a food intake-independent manner. These central effects are located in GABAergic neurons in the LHA and the neighbouring ZI. D2R triggers orexin signalling, which leads to decreased protein kinase A (PKA) activity, increased phosphodiesterase 3B (PDE3B)

and reduced ribosomal protein S6 (rpS6) levels. Of note, this thermogenic action depends on the sympathetic nervous system (SNS). Importantly, the clinical relevance of these findings is supported by the fact that patients treated with cabergoline for 12 months showed a significant weight loss, associated with augmented resting energy expenditure (REE), alongside metabolic improvement, through a prolactin-independent mechanism.

Results

Bromocriptine induces negative energy balance and thermogenesis. A single intracerebroventricular (ICV) injection of bromocriptine (40 and 80 μg per rat) significantly decreased body weight after 24 h independently of food or water intake, while a dose of 20 μg per rat did not change body weight (Supplementary Fig. 1a–d). The dose of 80 μg per rat elicited a significant early increase in food intake but after 24 h the food intake was similar between control and bromocriptine-treated animals. ICV injected bromocriptine-treated rats (40 μg per rat) showed increased energy expenditure (Supplementary Fig. 1e), BAT interscapular temperature (Supplementary Fig. 1f) and stimulation of 2-^{18}F-fluoro-2-deoxy-2-glucose (18F-FDG) uptake in BAT analysed by positron emission tomography-computed tomography (PET-CT) (Supplementary Fig. 1g); while no changes were found in body temperature or respiratory quotient (Supplementary Fig. 1h–i). Consistently, the analysis of histological sections revealed smaller lipid droplets in adipocytes of BAT from bromocriptine-treated rats (Supplementary Fig. 1j), increased BAT UCP1 protein levels (Supplementary Fig. 1k) and increased tolerance to cold exposure (Supplementary Fig. 1l). As expected, the central activation of D2R stimulated locomotor activity in the short-term (Supplementary Fig. 1m). To determine the relevance of physical activity on energy expenditure in relation to non-physical activity mechanisms (for example, resting metabolic rate), we performed correlations and found that energy expenditure and locomotor activity were positively correlated in the dark phase (right panel) but not in the light phase (left panel) (Supplementary Fig. 1n). In addition, we have also analysed energy expenditure (kcal h^{-1}) during 2 h of the light phase when animals were less active. During these 2 h of the light phase, we did not see any difference in energy expenditure between vehicle and bromocriptine-treated rats (Supplementary Fig. 1o), suggesting that bromocriptine does not affect resting metabolic rate. Bromocriptine and cabergoline are used in patients with prolactin-secreting pituitary adenomas[20], but circulating levels of prolactin in rats treated with ICV injected bromocriptine remained unchanged when compared to control groups (Supplementary Fig. 1p).

In addition, we injected prolactin ICV into male mice at two different doses (1 and 10 μg per mouse) and after 24 h (when bromocriptine caused a significant reduction in body weight independent of food intake), we failed to find any statistically significant effect on body weight and food intake (Supplementary Fig. 2a,b).

In keeping, prolactin ICV did not affect BAT interscapular temperature (Supplementary Fig. 2c). Overall, these results indicate that the central administration of prolactin does not alter BAT activity.

To rule out the possibility that centrally injected bromocriptine leaks out of the central nervous system (CNS) into the circulation and elicits a response by directly acting at a peripheral level, we administered bromocriptine peripherally, using the same dose as the one injected centrally. We were unable to detect changes in food intake, body weight or BAT temperature (Supplementary Fig. 3a–c). Consistent with this, when we injected an adenoviral vector encoding a short hairpin RNA (shRNA) against D2R in the BAT[21], the knockdown of D2R specifically in BAT (Supplementary Fig. 3d,e) did not prevent the effects of central bromocriptine on body weight (Supplementary Fig. 3f), food intake (Supplementary Fig. 3g), BAT interscapular temperature (Supplementary Fig. 3h) or BAT UCP1 levels (Supplementary Fig. 3i). In addition, to assess whether the effect of bromocriptine on BAT was sex-dependent or not, we injected a single ICV injection of bromocriptine (40 μg per rat) in females, and found that identically to males, it significantly decreased body weight and white fat mass after 24 h, concomitant with increased BAT interscapular temperature, and this effect was again independent of food intake (Supplementary Fig. 4a–e).

We next investigated if the effects of central bromocriptine may be long-lasting. Therefore, we chronically infused bromocriptine (40 μg per rat) over 2 weeks in rats fed a chow diet. We found that cumulative food intake remained unchanged, while body weight gain was significantly lower in rats treated with bromocriptine (Fig. 1a,b). Histological analyses revealed smaller lipid droplets in BAT of bromocriptine-treated rats, as well as an increased protein content of UCP1, FGF21 and PRDM16 (Fig. 1c,d). β-adrenergic receptors represent a key link involved in the regulation of adipose tissue metabolism by the SNS[22,23]. To determine whether the central bromocriptine action on BAT was mediated by the SNS, we injected the β3-adrenergic receptor-specific antagonist SR59230A (refs. [24,25]) and found that it reversed the effects of central bromocriptine on weight gain (Fig. 1a), BAT lipid content and BAT levels of thermogenic markers (Fig. 1c,d). After that, we assessed the efficacy of the chronic central infusion of bromocriptine in diet-induced obese (DIO) rats. Similarly, to the results obtained in rats fed a chow diet, central bromocriptine reduced body weight gain and adiposity in a feeding-independent manner (Fig. 1e–g). Consistently, energy expenditure was also higher (Fig. 1h), with changes neither in respiratory quotient nor locomotor activity (Fig. 1i,j). BAT from bromocriptine-treated DIO rats showed smaller lipid droplets and increased protein content of thermogenic markers (Fig. 1k,l). Moreover, the pharmacological blockade of the β receptor reversed the effects of central bromocriptine on weight gain, adiposity, energy expenditure, as well as BAT morphology and protein levels of UCP1 (Fig. 1f–l). To finally characterize the relevance of the SNS, triple knockout (TKO) (β1-, β2- and β3-adrenergic receptors) mice were

Fig. 1 | Chronic central infusion of bromocriptine reduces diet-induced obesity. a–d, Effects of a 14-d ICV infusion of bromocriptine (BC) (40 μg per rat, daily) and subcutaneous injection of SR59230A hydrochloride (3 mg kg^{-1}) on body weight (**a**); cumulative food intake ($n = 8$) (**b**); representative histology of BAT lipid content and quantification of lipid droplet average area ($n = 7$), scale bars, 200 μm (**c**); protein levels of BAT UCP1, FGF21, PRDM16 and PGC1α in rats fed a chow diet ($n = 7$) (**d**). **e–l**, Effect of a 10-d ICV infusion of BC (40 μg per rat, daily) and subcutaneous injection of SR59230A hydrochloride (3 mg kg^{-1}) on cumulative food intake (**e**); body weight change (**f**); white mass gain (**g**); energy expenditure (EE) (**h**); respiratory quotient (RQ) (**i**); locomotor activity ($n = 7$ vehicle, $n = 8$ BC and $n = 7$ BC + SR59230A hydrochloride treatment) (**j**); representative histology of BAT lipid content and quantification of lipid droplet average area ($n = 7$ each treatment), scale bars, 200 μm (**k**); protein levels of BAT UCP1, FGF21, PRDM16 and PGC1α ($n = 7$ vehicle, $n = 8$ BC and $n = 7$ BC + SR59230A hydrochloride treatment) in rats fed a HFD (**l**). **m–q**, Effect of a 7-d ICV infusion of BC (40 μg per mouse, daily) on body weight change (**m**); cumulative food intake (**n**); white mass change (**o**); representative histology of BAT lipid content and quantification of lipid droplet average area, scale bars, 200 μm (**p**); protein levels of BAT UCP1 ($n = 5$ WT vehicle and WT BC mice, $n = 4$ TKO vehicle and $n = 6$ TKO BC mice) (**q**). Protein data were expressed in relation (%) to control (vehicle-treated) animals. α-tubulin was used to normalize protein levels. Dividing lines indicate splicings within the same gel. Values are represented as the mean ± s.d. Statistical differences according to a one-way ANOVA followed by Bonferroni post hoc multiple comparison test (**a–c,e–k,j**), analysis of covariance (ANCOVA) with non-fat mass as covariate (**h**), or a Kruskal–Wallis followed by Dunn post hoc test for multiple comparisons (**d,e,l–q**). Values are represented as the mean ± s.e.m. *$P < 0.05$, **$P < 0.01$, ***$P < 0.001$ (**a,f,m**).

centrally infused with bromocriptine for 7 d. Bromocriptine did not affect food intake in WT or TKO mice, but significantly decreased body weight gain and white fat mass in WT mice, but not in TKO

mice (Fig. 1m–o). In agreement with this, central bromocriptine reduced BAT lipid content and increased BAT UCP1 protein levels in WT but not in TKO mice (Fig. 1p,q).
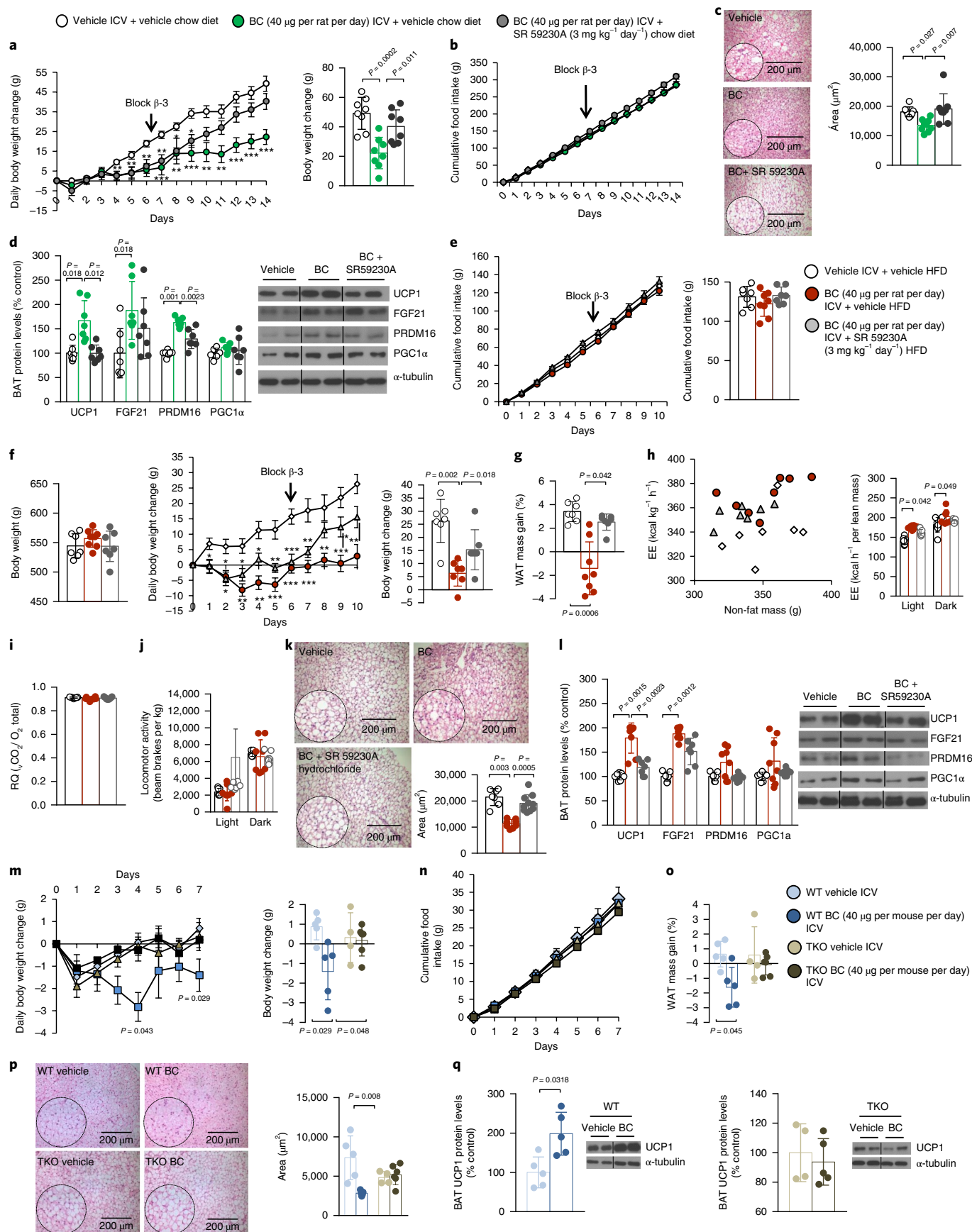
D2R in the LHA and ZI activates BAT in DIO rats. D2R is widely expressed in the hypothalamus[26]. Therefore, we examined the specific activation of the dopaminergic system in different hypothalamic sites. We found that a single injection of bromocriptine in the LHA and the ZI (Supplementary Fig. 4f) of rats fed a chow diet decreased body weight and stimulated BAT temperature after 24 h in a feeding-independent manner (Supplementary Fig. 4g–i). In these animals, circulating levels of prolactin did not change significantly compared to control groups (Supplementary Fig. 4j). When vehicle or bromocriptine were injected in the ventromedial nucleus (VMH) of rats fed a chow diet (Supplementary Fig. 4k), we found that the body weight of vehicle-treated rats decreased after 24 h, but bromocriptine-treated animals lost more weight and shower higher BAT temperature than controls independent of changes in feeding (Supplementary Fig. 4l–n). Notably, the central injection of bromocriptine in the LHA/ZI (Fig. 2a–e), but not within the VMH (Fig. 2f–h), of DIO rats reduced body weight, increased interscapular temperature, reduced the lipid content in BAT and increased BAT UCP1 protein levels without changing food intake (Fig. 2a–h).

We next used a designer receptor exclusively activated by designer drugs (DREADD) approach to specifically activate D2R neurons in the LHA and the ZI. D2R-cre mice fed a chow diet were bilaterally injected with AAV-hSyn-DIO-hM3D(Gq)-mCherry in the LHA and the ZI, where its expression was located (Fig. 2i). More specifically, D2R-mCherry neurons occupy the LHA area defined by the fornix/perifornical nucleus, the nigrostriatal bundle, cerebellar peduncle and the medial tuberal nucleus. After 3 weeks, activation of hM3D(Gq)-mCherry by intraperitoneal (i.p.) injections of clozapine-N-oxide (CNO) (1 mg kg⁻¹) leads to a decrease in body weight without changes in feeding and water intake (Fig. 2j,k). The decrease in body weight was associated with higher interscapular temperature, energy expenditure and BAT UCP1 protein levels, alongside decreased lipid content in BAT with unaltered body temperature, RQ, locomotor activity, resting metabolic rate or plasma prolactin levels (Fig. 2l–t). When animals were exposed to 4 °C, the group with D2R activated in the LHA/ZI showed a cold resistance as demonstrated by an increased capacity to maintain body and BAT temperature (Fig. 2u).

Since clozapine metabolite rather than CNO has been shown to mediate the activation of DREADD receptor after i.p. injection[27] and clozapine has some affinity with D2R, we also performed an independent experiment using this compound. Similar to CNO, the injection of clozapine decreased body weight and stimulated BAT temperature (Supplementary Fig. 4o,q). We next evaluated the phenotype of mice after the chemogenetic activation of D2R neurons at thermoneutrality (30 °C). At 30 °C, the activation of D2R neurons in the LHA and ZI resembled the effects found at 23 °C described above because the mice presented lower body weight, increased interscapular temperature and energy expenditure without changes in

body temperature or locomotor activity (Supplementary Fig. 5a–f). We also performed correlations between energy expenditure and locomotor activity but failed to find any correlation (Supplementary Fig. 5g). In addition, energy expenditure did not change during the 2 h of the light phase when animals were less active, suggesting that activation of D2R neurons in the LHA/ZI does not affect resting metabolic rate (Supplementary Fig. 5g).

To test whether D2R neurons located in other hypothalamic areas were also important for the regulation of BAT activity, we performed chemogenetic activation of D2R neurons in the mediobasal hypothalamus (MBH: arcuate nucleus (ARC) + VMH), including the tuberoinfundibular dopamine (TIDA) neurons controlling prolactin secretion from the anterior pituitary[28], and in the dorsomedial nucleus of hypothalamus (DMH). We found that chemogenetic activation of D2R neurons in the MBH and DMH did not affect body weight, interscapular temperature or white fat mass (Supplementary Fig. 6).

The effect of bromocriptine on BAT is dependent on D2R in the LHA/ZI. We stereotaxically delivered an adenoviral vector encoding a shRNA against D2R in the LHA/ZI in rats fed a chow diet. Infection efficiency in the LHA and ZI was assessed by expression of green fluorescent protein (GFP) and decreased levels of D2R (Fig. 3a,b). Although the selected titre of the adenoviral vector inhibiting D2R in the LHA/ZI did not affect either body weight or food intake, it attenuated bromocriptine-induced weight loss (Fig. 3c,d). In agreement with these results, the effect of bromocriptine on adiposity, BAT temperature, lipid content and UCP1 levels was absent when D2R was inhibited in the LHA/ZI (Fig. 3e–h). Furthermore, rats receiving bromocriptine in the LHA/ZI displayed a significant increase in c-FOS staining in the raphe pallidus (RPa) and the inferior olive (IO), which was indicative of higher neuronal activation (Fig. 3i).

However, the knockdown of D2R in the VMH (Supplementary Fig. 7a) of rats fed a chow diet did not ameliorate bromocriptine-induced weight loss, adiposity or interscapular temperature (Supplementary Fig. 7b–e). To further confirm the relevance of the LHA/ZI in the actions of bromocriptine, we performed another experiment injecting the adenoviral vector inhibiting D2R in the LHA/ZI (Supplementary Fig. 7f) and 2 weeks later, mice were treated with systemic bromocriptine at a dose higher than the one administered ICV. This i.p. dose (5 mg kg⁻¹) decreased body weight, WAT mass and activated BAT temperature and UCP1 protein levels (Supplementary Fig. 7g–k). However, these effects were completely abolished when the D2R was inhibited in the LHA/ZI (Supplementary Fig. 7g–k).

D2R action in GABAergic neurons requires orexin to modulate BAT. The LHA and the ZI are mainly composed of multiple neuronal populations expressing different neuropeptides and

Fig. 2 | Stimulation of D2R in the LHA/ZI stimulates BAT activity. a–e, Effect of specifically injecting BC (40 μg per rat) in the LHA/ZI on body weight change (**a**) and food intake (**b**) (n = 9 each treatment); infrared thermal images and quantification of BAT interscapular temperature (n = 5) (**c**); representative histology of BAT lipid content and quantification of lipid droplet average area (n = 5), scale bars, 200 μm (**d**); protein levels of BAT UCP1 (n = 7) after 24 h (**e**). **f–h,** Effect of specifically injecting BC (40 μg per rat) in the VMH on body weight change (**f**), food intake (**g**) and infrared thermal images and quantification of BAT interscapular temperature after 24 h (**h**) (n = 9 each treatment). **i,** Representative mCherry expression in the hypothalamic LHA/ZI after stereotaxic injection of hSYN-DIO-hM3D(Gq)-mCherry AVV, scale bar, 0.2 mm. **j,k,** Effect of the stereotaxic injection of hSYN-DIO-Hm3D(Gq)-mCherry AVV in the LHA/ZI of D2R-cre mice on body weight change (**j**), food intake and water intake (**k**). **l–u,,** Infrared thermal images and quantification of BAT interscapular temperature (**l**), and body temperature (n = 7 per group) (**m**); respiratory quotient (**n**); locomotor activity (**o**); energy expenditure (n = 5) (**p**); correlation between energy expenditure and locomotor activity in the dark phase, in the light phase and energy expenditure during 2 h of the light phase (Pearson correlation test) (**q**); representative histology of BAT lipid content (n = 6), scale bars, 200 μm (**r**); protein levels of BAT UCP1 (**s**); plasma prolactin levels (n = 7 vehicle and n = 6 CNO) after 24 h (**t**); and body temperature and BAT interscapular temperature in cold exposure (4 °C) (n = 9) (**u**). Protein data were expressed in relation (%) to control (vehicle-treated) animals. α-tubulin was used to normalize protein levels. Dividing lines indicate splicings within the same gel. The experiments were repeated five times (**i**). Data are mean ± s.d. Statistical differences according to a two-sided Student's t-test (**e–h,j,l,m,u**) or two-sided Mann–Whitney U-test (**a–d,k,n–s**).

neurotransmitters. To identify which neuronal populations were expressing D2R, we used a D2R-cre:Ribotag mouse line[29]. HA immunoreactivity allowing the identification of D2R-positive cells was detected in GABAergic and glutamatergic neurons in the LHA and the ZI, but not in cells expressing MCH or orexin (Fig. 3j). To discover the functional relevance of GABAergic and glutamatergic neurons in
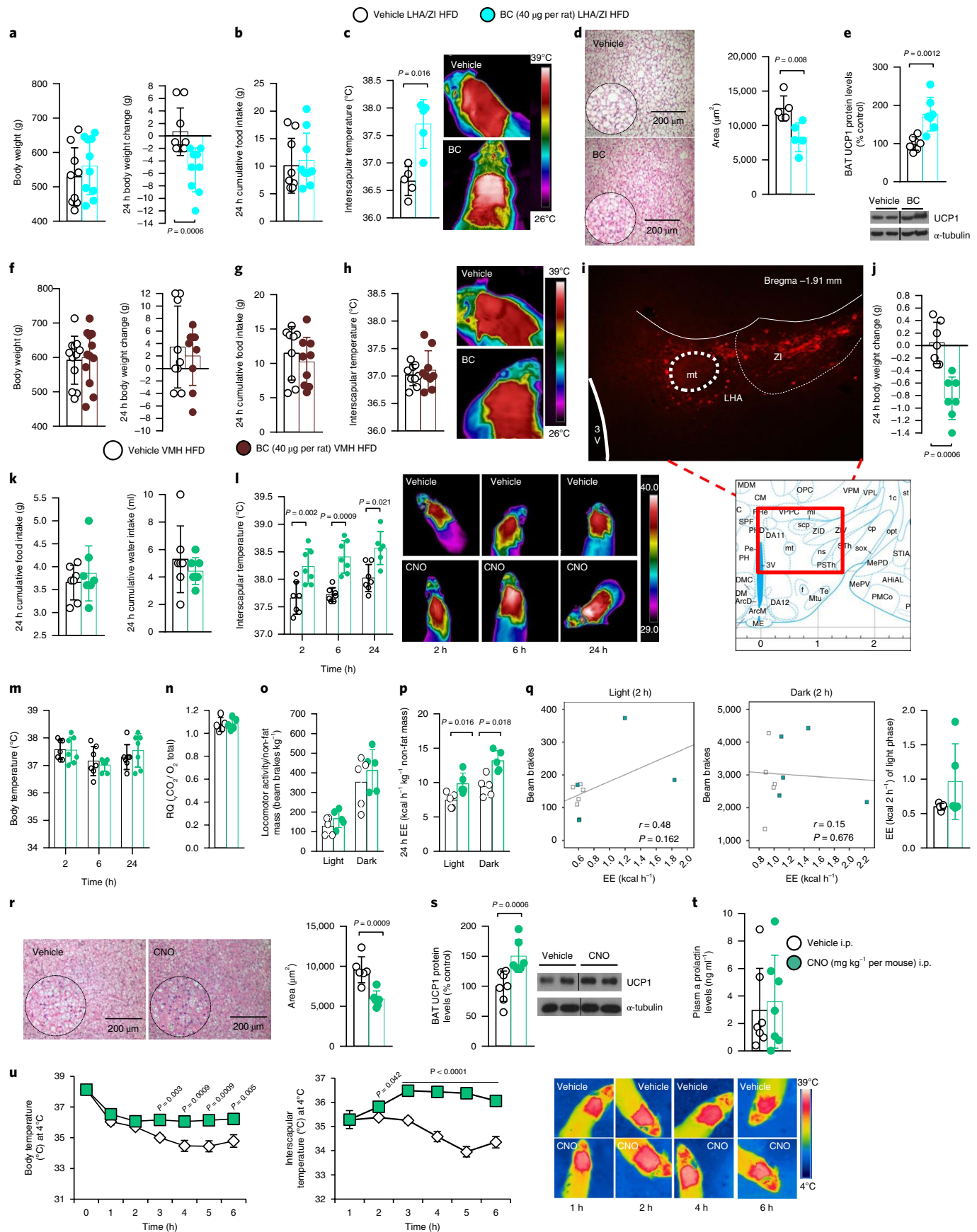
the actions of D2R, we over-expressed D2R in these neuronal populations injecting a viral vector (Ad-hSyn-DIO-D2R) in the LHA/ZI of Vglut2-ires-cre and Vgat-ires-cre mice. Fluorescent activated cell sorting (FACS) demonstrated that the virus targeted 198.2 ± 10.2 cells per animal in the LHA/ZI and confirmed D2R expression in GABAergic and glutamatergic neurons (Fig. 4g). The gating strategy for FACS is detailed in Supplementary Fig 8. We found that overexpression of D2R in GABAergic (Fig. 4f–k), but not glutamatergic cells of the LHA/ZI (Fig. 4a–e), reduced body weight and increased interscapular temperature and UCP1 protein levels independent of food intake. In line with this, the inhibition of D2R in GABAergic neurons of the LHA/ZI using a viral vector expressing a shRNA against D2R (Ad-hSyn-DIO-shD2R) increased body weight and decreased interscapular temperature when compared to control mice (Fig. 4l–o).

Since GABA regulates the activity of different neuronal populations in the LHA, we next tested whether the effects of the hypothalamic dopamine system required orexin or MCH, two neuropeptides known to be involved in thermoregulation[30,31]. We found that bromocriptine administered ICV increased orexin, but not MCH, messenger RNA levels in the LHA (Supplementary Fig. 9a). Similarly, bromocriptine directly injected in the LHA/ZI augmented orexin protein levels (Supplementary Fig. 9b), the knockdown of D2R in the LHA/ZI prevented bromocriptine-induced orexin protein levels (Supplementary Fig. 9c), and the chemogenetic activation of D2R in LHA/ZI stimulated orexin levels (Supplementary Fig. 9d). The specific isolation of the LHA/ZI was corroborated by measuring protein levels of orexin and MCH, which are specifically located in the LHA and were not detected in the VMH (Supplementary Fig. 9e). There are no specific markers for the ZI. The isolated micropunches included the LHA and the ZI because, due to their neighbouring localization and the lack of specific markers, it is virtually impossible to separate the ZI from the LHA. Moreover, the specificity of the antibodies for D2R, orexin and MCH were tested in D2R null mice, orexin null mice and rats injected with an MCH antisense oligonucleotide, respectively (Supplementary Fig. 10a).

To investigate the mechanistic link between LHA D2R and the orexin system, we next assessed the effects of central bromocriptine in mice lacking orexin. We found that while bromocriptine decreased body weight in a food-independent manner, increased interscapular temperature, decreased lipid content in BAT and up-regulated BAT UCP1 protein levels in WT mice it was unable to exert these actions in orexin-deficient mice (Fig. 4p–t).

To further characterize the role of orexin as a mediator of dopamine actions, we performed chemogenetic stimulation of D2R neurons in the LHA/ZI and concomitant treatment with the orexin receptor 1 antagonist SB-334867 (ref. [32]). Our findings demonstrated that the effects of D2R activation in the LHA/ZI on body weight, interscapular temperature, BAT lipid content and UCP1 levels were completely blocked when SB-334867 was injected ICV (Fig. 4u–x).

PDE3B and PKA mediate the actions of bromocriptine. PKA signalling has been related to non-metabolic dopamine D2R actions in some extrahypothalamic areas[33,34]. Herein, we measured phosphorylated cAMP response element-binding protein (pCREB) as a marker of PKA activity[35]. We found that both bromocriptine administered either ICV or in the LHA/ZI (Fig. 5a,b) and chemogenetic activation of D2R in the LHA/ZI (Fig. 5c) decreased pCREB protein levels, an effect that was blunted by the injection of the orexin receptor 1 antagonist (Fig. 5c). This decrease in pCREB levels was also detected after the injection of orexin A, an effect blocked by the orexin receptor 1 antagonist (Fig. 5d). Thus, these data indicate that both bromocriptine and orexin modulate PKA activity.

Central injection of the specific PKA activator Sp-cAMPS (90 ng per rat)[35,36], abolished the effects of bromocriptine on body weight, white mass, BAT interscapular temperature, lipid content and UCP1 protein levels in a feeding-independent manner after 24 h (Fig. 5e–j). Furthermore, the administration of the PKA inhibitor H-89 (62 ng per rat)[35,36] in the LHA/ZI recapitulated the effects of bromocriptine, since it decreased body weight, white mass and BAT lipid content and stimulated BAT interscapular temperature and UCP1 protein levels (Fig. 5k–p) independent of food intake.

Phosphodiesterases (PDEs) are enzymes that break a phosphodiester bond and are classified in different families. PDE3 is highly sensitive to the inhibition of cAMP hydrolysis by cGMP, and there are 2 PDE3 isoforms that are encoded by different genes (PDE3A and PDE3B)[37]. Hypothalamic PDE3B was found to play a relevant role in regulating the action of leptin on feeding[38] and insulin[39]. PDE3B is also related to hypothalamic leptin signalling during the development of diet-induced obesity[40]. We measured protein levels of PDE3B in the LHA/ZI of mice and found that after the chemogenetic stimulation of D2R in this hypothalamic area, PDE3B levels were increased compared to control mice (Fig. 5q). Then, we injected ICV the PDE3 inhibitor cilostamide at a reported dose (10 μg per mouse)[39] that did not affect body weight or food intake (Fig. 5r,s). However, this dose of cilostamide blocked the effects of chemogenetic activation of D2R on body weight and interscapular temperature (Fig. 5t–v). Finally, we injected cilostamide ICV in mice where D2R was over-expressed in GABA neurons injecting the Ad-hSyn-DIO-D2R in the LHA/ZI of Vgat-ires-cre mice; our data showed that cilostamide ameliorated the suppression of body weight and stimulation of BAT activity and increased energy expenditure induced by D2R overexpression in GABA neurons (Fig. 5w–z). Overall, these results indicate that PDE3B mediates the central effects of the hypothalamic dopamine system within LHA/ZI on body weight and BAT activity.

rpS6 in the LHA/ZI modulates the actions of bromocriptine. PKA is known to regulate rpS6 (refs. [41,42]). Thereby, we investigated the possibility that rpS6 was mediating the actions of bromocriptine on energy balance. Phosphorylated levels of rpS6 (P-rpS6) were significantly decreased after the injection of bromocriptine ICV (Fig. 6a,b) or in the LHA/ZI (Fig. 6c), an effect that was blunted when D2R was knocked down specifically in the LHA/ZI (Fig. 6d) and when bromocriptine was injected in orexin-deficient mice (Fig. 6e). The chemogenetic activation of D2R in the LHA/ZI also resulted in

Fig. 3 | Knockdown of D2R in the LHA/ZI blunts bromocriptine-induced weight loss. a, Representative photomicrograph of brain section showing the injection of the viral vectors that encode GFP expression precisely placed in the LHA/ZI, scale bar, 0.1 mm, and, **b**, D2R protein levels in the LHA/ZI 3 weeks after the viral infection ($n=7$ per group). **c–i**, Effect of injecting adenoviral particles encoding for GFP- or D2R-KD in the LHA/ZI of rats treated with ICV BC (40 μg per rat) on body weight change (**c**), food intake (**d**), White adipose tissue (WAT) weight (**e**) and infrared thermal images and quantification of BAT interscapular temperature (**f**) ($n=6$ GFP vehicle, $n=8$ GFP BC, $n=9$ D2R-KD vehicle and $n=9$ D2R-KD BC); representative histology of BAT lipid content and quantification of lipid droplet average area ($n=5$) scale bars, 200 μm (**g**); BAT UCP1 protein levels ($n=6$ in each treatment) (**h**); c-FOS immunoreactive cells (IR) in the rRPa and IO with representative sections (Gi, gigantocellular reticular nucleus; IO, inferior olive; py, pyramidal tract; RPa, raphe pallidus; scale bar, 100 μm ($n=5$) (**i**). **j**, Double immunostaining of HA and orexin, MCH, Vgat and Vglut2 in D2R-cre:Ribotag mice, scale bars, 100 μm; insets, 40 μm; high magnification, 8 μm. Yellow arrows indicate neurons with colocalized HA and MCH. α-tubulin and β-actin were used to normalize protein levels. Protein data were expressed in relation (%) to control (vehicle-treated) animals. Dividing lines indicate splicings within the same gel. The experiments were repeated six times (**a,j**). Data are mean ± s.d. Statistical differences on the basis of a one-way ANOVA followed by Bonferroni post hoc multiple comparison test (**c,d,f,g**) or two-tailed Student´s t-test (**b,e,h,i**).

lower P-rpS6 protein levels, and this effect was prevented by the antagonism of orexin receptor 1 (Fig. 6f). In line with this, orexin, which also down-regulates P-rpS6 levels failed to do that when the orexin receptor 1 antagonist was given (Fig. 6g). These results suggest that both D2R and orexin signalling were important for the

modulation of P-rpS6. Importantly, the effects of bromocriptine on P-rpS6 were specific, because when we measured hypothalamic protein levels of multiple molecules known to have important effects on energy homeostasis such as phosphorylated c-Jun N-terminal kinase (pJNK), JNK, phosphorylated protein kinase B (pAKT), AKT or
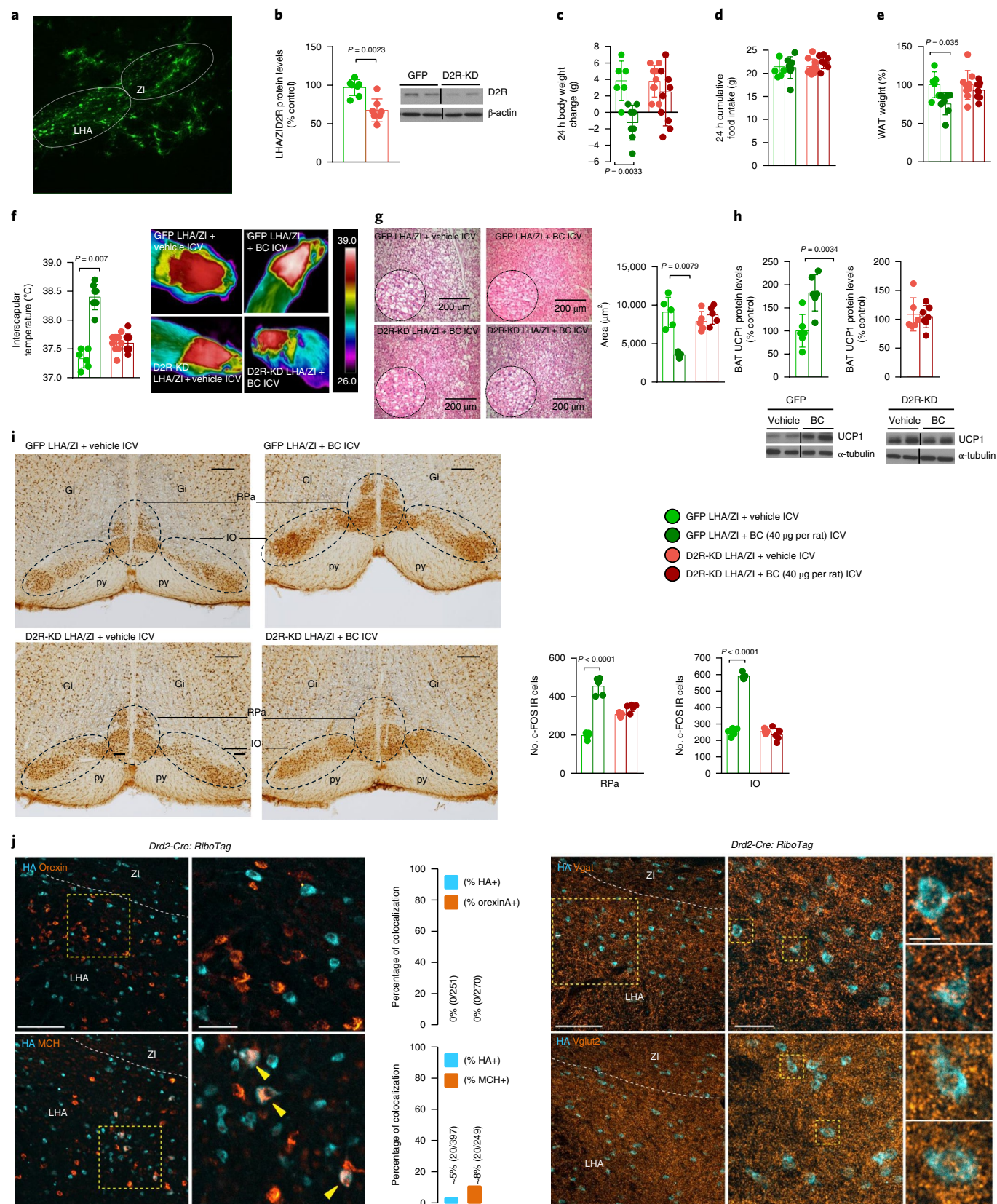
mammalian target of rapamycin (mTOR), they remained unaltered after bromocriptine treatment (Supplementary Fig. 10b). In addition, we found that the administration of H-89 in the LHA/ZI decreased P-rpS6 levels (Fig. 6h) and that the activation of PKA by Sp-cAMPS blunted bromocriptine-induced rpS6 inhibition (Fig. 6i).

Given that rpS6 was regulated by bromocriptine/orexin/PKA, we next performed a functional study using adenovirus encoding a constitutively active form of S6K (CA-S6K-Ad)[43] in the LHA/ZI. We confirmed the efficiency of the viral vector by detecting increased P-rpS6 protein levels 8 d after the stereotaxic administration of CA-S6K-Ad (Fig. 6j). Although the dose of the adenoviral vector activating S6K in the LHA/ZI did not affect food intake or body weight, it attenuated bromocriptine-induced weight loss (Fig. 6k,l), the increase in interscapular temperature (Fig. 6m), the reduction of lipid content in BAT (Fig. 6n) and the up-regulation of BAT UCP1 (Fig. 6o). To note, the activation of S6K did not modify the bromocriptine-induced orexin levels in the LHA/ZI, confirming that rpS6 is downstream orexin (Ad Null LHA/ZI + vehicle ICV: 100 ± 9.1, Ad Null LHA/ZI + bromocriptine (40 ug per rat) ICV: 136.7 ± 9.6, Ad S6K1 LHA/ZI + vehicle ICV:104.0 ± 8.9, Ad S6K1 LHA/ZI + bromocriptine (40 ug per rat) ICV: 126.2 ± 6.8).

Dopamine agonism decreases body weight in patients with hyperprolactinemia. In the retrospective study after one year of cabergoline treatment instauration with 0.5 mg twice weekly all patients normalized the hyperprolactinemia irrespective of sex. Side effects were infrequent and very mild (nausea and postural hypotension) and no patient was withdrawn from the treatment for this reason. A statistically significant decrease in body weight and body mass index (BMI) were observed (Table 1 and Fig. 7a). Note that a huge inter-individual variability in weight loss was evident (Fig. 7a). Of interest, after 12 months of cabergoline treatment, a statistical improvement in glucose metabolism as evidenced by decreases in glucose and insulin concentrations as well as in the homeostatic model assessment insulin resistance (HOMA-IR) index was observed. The same was true for the lipid profile with significant reductions in the levels of triglycerides, total and LDL cholesterol. No sex differences were observed with regards to both the anthropometric and metabolic changes.

Dopamine agonism increases energy expenditure in patients with hyperprolactinemia. To gain more insight into the potential impact of dopamine agonism on body weight, body composition, REE and metabolic changes were analysed in a prospective study in patients with hyperprolactinemia. As observed in the retrospective study one year after cabergoline treatment instauration with 0.5 mg twice weekly all patients normalized the hyperprolactinemia irrespective of sex. Side effects were again infrequent and very

mild (nausea, postural hypotension and dizziness) with no patient withdrawing from the treatment. In this case, the statistically significant reduction in body weight and BMI was already observed after 3 months of cabergoline treatment (Fig. 7b) and persisted after 12 months (Table 1). Again, patients exhibited a huge inter-individual variability in weight loss both after 3 and 12 months following cabergoline treatment irrespective of the weight category (Fig. 7b). The magnitude of weight loss was greater after 3 months when compared to 12 months. Note, following cabergoline treatment body composition analysis showed a significant decrease of both total and visceral adiposity as evidenced by reduction of body fat percentage and waist circumference, respectively (Table 1). In line with the anthropometric changes observed, a statistically significant increase in REE was documented expressed in absolute terms or adjusted by either total body weight or fat-free mass. Importantly, patients showed the REE predicted from the Harris–Benedict equation before starting the cabergoline treatment, however after 3 months of treatment the REE was significantly higher than the theoretical REE (Fig. 7c); and there was a positive correlation between the REE adjusted per body weight after cabergoline treatment and weight loss (Fig. 7d). Cabergoline treatment was followed by a significant improvement in glucose metabolism as evidenced by decreases in glucose and insulin concentrations as well as in the insulin resistance HOMA-IR index, which was already evident after 3 months. Triglyceride concentrations also significantly decreased after 3 and 12 months of cabergoline, although in this case no changes in total, low-density lipoprotein (LDL) and high-density lipoprotein (HDL) cholesterol levels were observed. As in the retrospective study, no significant differences in the anthropometric, REE and metabolic effects between men and women took place.

Discussion

Our findings indicate that the brain dopamine system directly activates BAT thermogenesis in a feeding-independent manner. More specifically, these actions are mediated by the stimulation of D2R in GABAergic neurons located within the LHA and the ZI, which activates the SNS and ultimately leads to the increase of UCP1, BAT temperature and energy expenditure. This process is mediated by the up-regulation of orexin and PDE3B, which in turn decreases cAMP and the activity of PKA and rpS6. These findings provide information about the brain site and mechanisms by which fat mass decreases in response to the stimulation of CNS D2R activity, independently of anorexigenic actions. We also observed that patients treated with cabergoline, a D2R agonist, for 12 months showed a reduction in BMI and body fat together with an increase in REE and an improvement in glucose and lipid metabolism.

The mechanisms by which central dopamine affects body weight are widely assumed to be related to food intake and reward[17,44].

Fig. 4 | D2R action in GABAergic neurons requires orexin to modulate BAT. a, Photomicrograph showing the colocalization of GFP and Vglut2 in the LHA/ZI. **b–e**, Effect of injecting Ad-hSyn-DIO-EGFP or Ad-hSyn-DIO-D2R-EGFP in the LHA/ZI of vglut2-ires-cre mice on body weight change (**b**), food intake (**c**), BAT temperature (**d**) ($n = 10$) and BAT UCP1 protein levels (**e**) ($n = 4$). **f**, Photomicrograph showing the colocalization of GFP and Vgat in the LHA/ZI. **g**, Profiles from sorted non-infected/EGFP (cortex) and infected/EGFP sites (hypothalamus) and mRNA expression of Vgat, Vglut2 and Drd2 in Vgat-ires and Vglut2-ires-cre mice injected with Ad-hSyn-DIO-EGFP in the LHA/ZI ($n = 4$). **h–k**, Effect of injecting Ad-hSyn-DIO-EGFP or Ad-hSyn-DIO-D2R-EGFP in the LHA/ZI of vgat-ires-cre mice on body weight change (**h**), food intake (**i**), BAT temperature (**j**) ($n = 12$) and BAT UCP1 protein levels (**k**) ($n = 4$). **l–o**, Effect of injecting the Ad-hSyn-DIO- EGFP or Ad-hSyn-DIO-shD2R-EGFP in the LHA/ZI of vgat-ires-cre mice on body weight change (**l**), food intake (**m**) ($n = 7$), BAT temperature (**n**) and BAT UCP1 protein levels (**o**) ($n = 6$). **p–t**, Effect of a 24-h ICV injection of bromocriptine (BC) (40 µg) on body weight change (**p**), food intake (**q**), infrared thermal images and quantification of BAT temperature (**r**), histology of BAT lipid content and quantification of lipid droplet average area (**s**) ($n = 4$); and BAT UCP1 protein levels (**t**) in WT ($n = 4$) and orexin knockout ($n = 6$) mice. **u–x**, Effect of injecting of AAV-hSYN-DIO-Hm3D(Gq)-mCherry and the ICV injection of the orexin receptor antagonist SB-334867 (4 µg) on body weight change (**u**) and infrared thermal images and quantification of BAT temperature (**v**) ($n = 5–6$); histology of BAT lipid content and quantification of lipid droplet average area (**w**) and immunostaining of UCP1 and quantification in BAT (**x**) ($n = 8$) after 24 h. Dividing lines indicate splicings within the same gel. α-tubulin was used to normalize protein levels. The experiments were repeated six times (**a,h**). Data are mean ± s.d. Statistical differences on the basis of a two-tailed Student´s t-test (**b–d,h–k**), a Kruskal–Wallis followed by Dunn post hoc test for multiple comparison (**c,p,q**), two-way ANOVA (**r**), two-sided Mann–Whitney U-test (**e,g,l–o,s,t**) or a one-way ANOVA followed by Bonferroni post hoc multiple comparison test (**u–x**).

Within the hypothalamus, dopamine levels in the LHA immediately increase in response to feeding and normalize after meal consumption[45–47], and injection of D2R antagonists in the LHA reverses amphetamine-induced anorexia[48,49]. However, dopamine levels in the VMH decrease after feeding and increase during fasting[50] and dopamine injection in this area increased meal size while decreasing
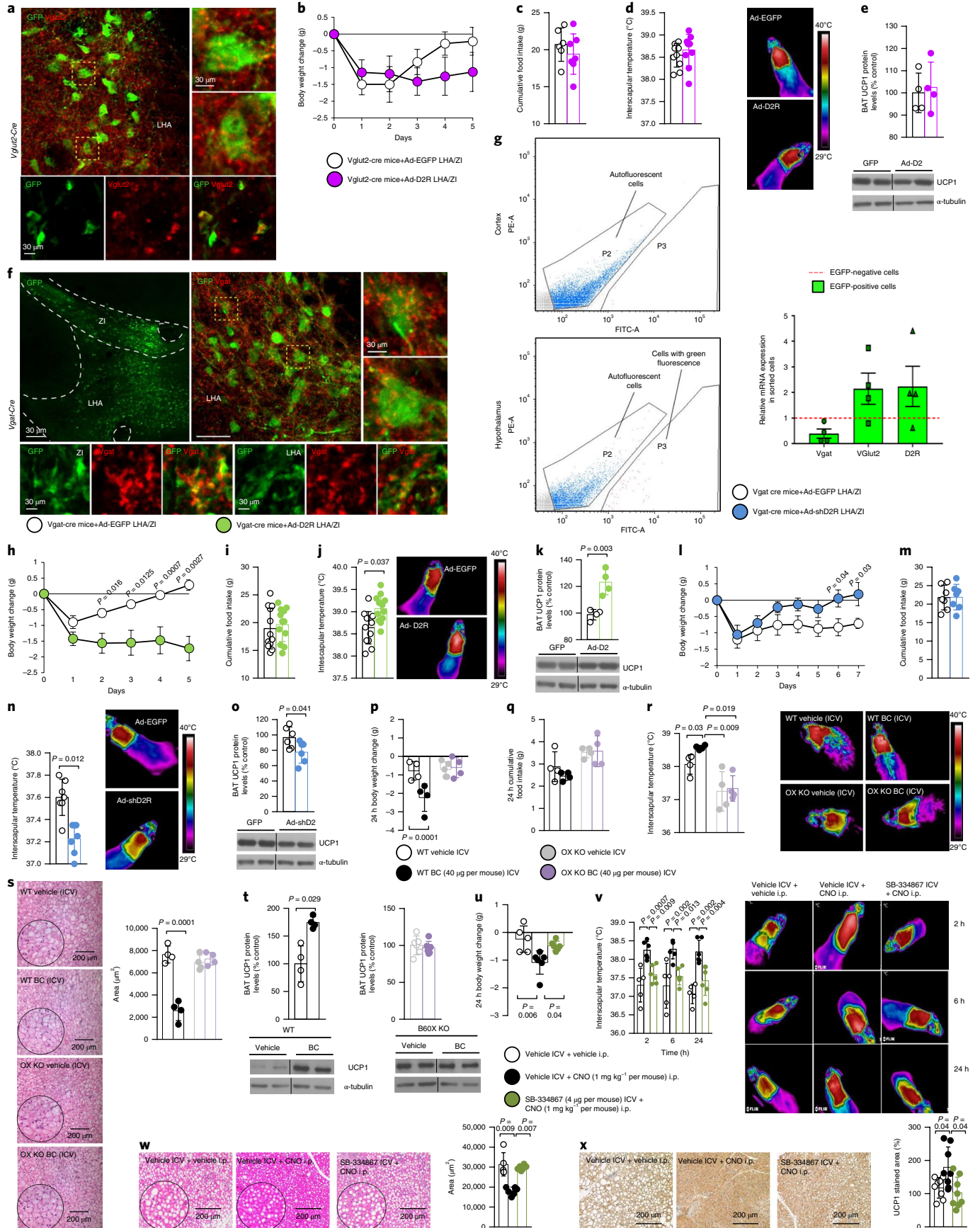
meal number[51]. In line with this, tyrosine hydroxylase neurons of the ARC excited AgRP neurons and inhibited POMC neurons, suggesting that dopamine has anorexigenic action in this hypothalamic site[52]. More recently, one report has shown that activation of striatal D2R reduced BAT thermogenesis and energy expenditure, and accelerated obesity despite reduced eating[53]. The study supported the idea that the dopamine system may exert different actions depending on the hypothalamic site. Nevertheless, some reports showed that although chronic obesogenic diets reduce striatal D2R function, striatal D2R down-regulation does not lead to obesity[54,55], suggesting that changes in striatal D2R expression could be a consequence rather than the cause of obesity.

In addition to the well-known effects on food intake, the hypothalamic areas where D2R is highly expressed, are also important centres for the control of BAT activity[56]. Therefore, we hypothesized that D2R stimulation at this level could trigger BAT thermogenesis. We found that chronic central infusion of bromocriptine increases BAT activity and ameliorates diet-induced obesity, independently of feeding. These effects are regulated by the SNS since its pharmacological or genetic disruption blunts bromocriptine-induced effects on BAT. The hypothalamic area responsible for the effects of bromocriptine resides in the LHA and the ZI because pharmacological and chemogenetic stimulation of D2R in these areas reduces HFD-induced adiposity due to increased BAT activity and higher energy expenditure. The chemogenetic stimulation of D2R neurons in the LHA/ZI, but not in the VMH or DMH, also stimulated BAT activity and decreased adiposity in conditions of thermoneutrality. Supporting these data, the loss-of-function of D2R by shRNA in the LHA/ZI was enough to block the actions of central and peripheral bromocriptine on BAT function. Therefore, these results indicate that the site of action of the dopamine system to regulate BAT activity occurs specifically in the LHA/ZI but not in other hypothalamic regions.

In line with this, even though dopamine receptors have been detected in brown adipocytes and dopamine stimulates thermogenesis in these cells[57], when we inhibited D2R in BAT, central bromocriptine was still able to decrease body weight and increase BAT temperature. Overall, our in vivo results indicate that the thermogenic action of bromocriptine requires the presence of D2R in the LHA/ZI, while D2Rs located in BAT are not necessary. Previous reports have suggested that the effects on food intake occur in the ARC and VMH and our present findings indicate that chemogenetic activation of D2R in the MBH, which includes ARC and VMH, or in the DMH, does not affect BAT thermogenesis while D2R neurons in the LHA and ZI regulate BAT and increase energy expenditure. Therefore, the effects of dopamine on food intake from those on energy expenditure are dissociated since dopamine requires the ARC to regulate food intake[52] and the present study indicates that dopamine actions in the LHA and ZI control BAT activity and energy expenditure.

The LHA and ZI are heterogeneous brain areas containing numerous genetically distinct cell populations that use a plethora of signalling mechanisms. Our findings indicate that D2R is located in both glutamatergic and GABAergic cells, but only genetic manipulation of D2R in GABAergic neurons exert marked effects on body weight. This is of relevance because both GABA neurons and dopamine modulate orexin activity[58,59]. A key role of orexin is related to energy expenditure via the regulation of thermogenesis[31,32,60,61]. However, despite these data, it was totally unknown whether the interaction with the central dopamine system could play a significant role in energy homeostasis. To address that possibility, we investigated whether the central thermogenic effect of bromocriptine was associated with orexin function. Our findings indicate that central stimulation of D2R increased orexin expression and that bromocriptine failed to activate BAT thermogenesis in orexin-deficient mice. In agreement with this, the effect of the chemogenetic stimulation of D2R neurons in the LHA/ZI was blunted after the central blockade of the OX1R. Thus, our results indicate that orexin mediates the thermogenic effects of brain D2R stimulation.

Dopamine has been related with cAMP-dependent signalling. More precisely, the activation of D2R inhibits[62] while the D2R antagonist haloperidol promotes the stimulation of cAMP-dependent PKA and increased the phosphorylation of rpS6 in neurons of the striatum[42]. Moreover, PDE and more precisely PDE3B is highly sensitive to inhibition of cAMP hydrolysis by cGMP[37]. Hypothalamic PDE3B plays a relevant role in regulating the action of leptin[38] and insulin[39]. Our results indicate that PDE3B mediates the central effects of the dopamine system on body weight and BAT activity. Thus, our current model is that high levels of PDE3B degrade cAMP and these low levels of cAMP subsequently determine the low activity of PKA. Hypothalamic PKA[35,63] and rpS6[43] have been reported to play a relevant role in the control of energy balance, but their role within the LHA is still unexplored. Furthermore, PKA has been identified as a regulator of rpS6 in neuronal cells[42]. Therefore, we hypothesized that bromocriptine might be using this pathway in the LHA to exert its actions on BAT. Our findings demonstrate that both pharmacological and chemogenetic activation of D2R decreased PKA activity, measured by the surrogate marker pCREB. Accordingly, the direct injection of the PKA inhibitor named H-89 in the LHA/ZI stimulated BAT activity and decreased body weight, and the activation of PKA by Sp-cAMPS totally blunted bromocriptine effects on weight loss, BAT temperature and UCP1 expression. Overall, these results indicate that bromocriptine-mediated actions on BAT activity are mediated by PKA-catalysed phosphorylation of rpS6. In line with our findings, previous studies have shown that the inactivation of central PKA, achieved by the disruption of several of its subunits causes resistance to diet-induced obesity[64,65]. However, our study addresses the relevant role of PKA in the LHA/ZI.

In line with the findings made in rodents, dopamine agonism in both our retrospective and prospective studies of patients with

Fig. 5 | PKA mediates the effects of bromocriptine on BAT. a–d, Phosphorylated levels of CREB in the LHA/ZI after 2-h ICV (**a**) and 24-h specific injection of BC (40 µg) in the LHA/ZI (*n* = 7) (**b**); injection of AAV-hSYN-DIO-hM3D (Gq)-mCherry and the ICV injection of SB-334867 (4 µg) (*n* = 5–6) (**c**); ICV injection of orexin (OX) (10 µg) and SB-334867 (4 µg) after 24 h (*n* = 5–9) (**d**). **e–j**, Effect of the ICV injection of BC (40 µg) and Sp-cAMPS (90 ng) on body weight change (**e**), food intake (**f**) and white mass gain (**g**) (*n* = 9); and BAT temperature (**h**) (*n* = 7–8). **i**, Histology of BAT lipid content and quantification of lipid droplet area. **j**, Immunostaining of UCP1 and quantification in BAT (*n* = 7) after 24 h. **k–p**, Effect of the LHA/ZI injection of the specific PKA inhibitor H-89 (62 ng) on body weight change (**k**), food intake (**l**), white mass gain (**m**) and BAT temperature (**n**) (*n* = 11–12); histology of BAT lipid content and quantification of lipid droplet area (*n* = 10) (**o**); protein levels of BAT UCP1 (*n* = 7) after 24 h (**p**). **q**, Effect of the injection of AAV-hSyn-DIO-hM3D (Gq)-mCherry in the LHA/ZI of D2R-cre mice on PDE3B levels in the LHA/ZI (*n* = 6). **r,s**, Effect of the ICV injection of cilostamide (10 µg) on body weight (**r**) and food intake (**s**) (*n* = 7). **t–v**, Effect of the injection of AAV-hSyn-DIO-Hm3D (Gq)-mCherry in the LHA/ZI of D2R-cre mice and the ICV injection of cilostamide (10 µg) on body weight (**t**), food intake (**u**) and BAT temperature (**v**) (*n* = 6). **w–z**, Effect of the injection of Ad-hSyn-DIO-EGFP or Ad-hSyn-DIO-D2R-EGFP in the LHA/ZI of Vgat-ires-cre mice and ICV cilostamide (10 µg) on body weight (**w**), food intake (**x**), BAT temperature (**y**) and energy expenditure (EE) after 24 h (**z**) (*n* = 7–8). Dividing lines indicate splicings within the same gel. α-tubulin, β-actin and GAPDH were used to normalize protein levels. Data are mean ± s.d. Statistical differences according to a two-tailed Student´s *t*-test (**a,b,q–s**), a one-way ANOVA followed by Bonferroni post hoc multiple comparison test (**c,e–j,w–y**), a Kruskal–Wallis followed by Dunn post hoc test for multiple comparison (**d,t–v**,) or two-sided Mann–Whitney *U*-test (**k–p**) and ANCOVA with body weight as covariate (**z**).

hyperprolactinemia have decreased body weight and improved glucose and lipid metabolism. The weight loss was accompanied by a reduction in both total body fat and visceral adiposity. Interestingly,

dopamine agonism achieved by cabergoline treatment in patients with hyperprolactinemia resulted in an increase in REE that is consistent with the bromocriptine-induced effects on BAT observed in

rodents. Moreover, in patients treated with cabergoline, the weight loss is positively correlated to REE. Our observations are in agreement with previous studies of bromocriptine or cabergoline treated patients[66–68]. Note, while cabergoline decreases body weight in both lean and overweight patients irrespective of BMI a clear variability in this response is observed, and patients with higher BMIs are in a position of losing more excess weight. Our preclinical studies indicate that prolactin is not mediating the effects of bromocriptine nor chemogenetic manipulation of neuroendocrine TIDA neurons on body weight and BAT activity. In line with this, in human studies, it is unlikely that weight loss is secondary to the normalization of prolactin because all the patients with prolactinomas treated with cabergoline showed a normalization in prolactin levels. Despite normalized prolactin levels in all the patients treated with cabergoline, they showed changes in body weight. Therefore, there is no correlation between circulating prolactin levels and body weight.

In summary, this study reveals that the activation of D2R in GABA neurons within the LHA and ZI stimulates orexin and PDE3B, which lowers cAMP levels and inhibits a PKA-rpS6. This increases SNS tone, upregulates BAT thermogenesis and increases energy expenditure, leading to weight loss. In line with this, patients undergoing treatment with the dopamine agonist cabergoline experienced an increase in energy expenditure, leading to total body weight and fat loss. Therefore, this study provides mechanistic insight into the mechanisms taking place at the CNS by which bromocriptine/cabergoline exert their beneficial effects on energy balance and metabolic homeostasis in a clinical setting.

Methods

Animals and diets. Male and female Sprague-Dawley rats (200–250 g); wild type (WT) and triple β-adrenoreceptor (AR) knockout (TKO) male mice (weight 20–25 g, age 8–10 weeks old)[69,70]; WT and orexin knockout male mice (null *Ox/Hcrt* mice, *orexin/hypocretin*; B6.129S6-Hcrttm1Ywa/J, The Jackson Laboratory) (weight 25–30 g, age 10–12 weeks old)[32], WT and Drd2-cre male mice (C57BL/6J, weight 20–25 g, age 8–10 weeks old)[71], Drd2-cre:riboatg mice (weight 25–30 g, age 8–10 weeks old)[29], vgat-ires-cre knock-in (C57BL/6J) and vglut2-ires-cre knock-in (C57BL/6J) from the Jackson Laboratory (weight 20–25 g, age 8–10 weeks old) were used for the experiments and littermates controls were used in each experiment (Reporting Summary). Except for Drd2-cre:Ribotag mice, all animals were housed in individual cages under controlled conditions of illumination (12 h light:dark cycle), temperature and humidity. The animals were allowed free access to water and a standard laboratory diet (CD) (Scientific Animal Food & Engineering, proteins 16%, carbohydrates 60% and fat 3%) or a high fat diet (HFD) (Research Diets 12492; 60% of calories from fat, 5.24 kcal g⁻¹; Research Diets) for 12 weeks. Food intake and body weight were measured daily during the experimental phase in all experiments. There were 4 to 12 animals per group. The animals were euthanized, and all the tissues were removed rapidly, frozen immediately on dry ice and kept at −80 °C until analysis. All experiments and procedures involved in this study were reviewed and approved by the Ethics Committee of the University of Santiago de Compostela, in accordance with European Union normative for the use of experimental animals.

Body composition and indirect calorimetry. Body composition (white fat mass) was measured using a nuclear magnetic resonance system (Whole-Body Composition Analyzer; EchoMRI). Measurements were performed before surgery and on the last day of the treatment. Energy expenditure, respiratory quotient and locomotor activity were assessed using a calorimetry system (LabMaster; TSE Systems)[24,72].

Temperature measurements, thermal imaging, cold exposure and thermoneutrality. Interscapular temperature was assessed and was visualized using a high-resolution infrared camera (E60bx: Compact-Infrared-Thermal Imaging-Camera; FLIR) and analysed with a FLIR-Tools specific software package[73]. Body temperature was recorded with a rectal probe connected to a digital thermometer (BAT-12 Microprobe-Thermometer; Physitemp). After the acute injection of bromocriptine, rats were placed for 6 h in a special room with a stable temperature of 4 °C (ref. [74]). D2r-cre mice were moved to a thermoneutral environment (30 °C with relative humidity of 45–52%) to eliminate the extrametabolism needed to defend the body temperature at lower temperatures[75].

ICV treatments. Animals were anaesthetized by an i.p. injection of a ketamine-xylazine mixture (ketamine 100 mg kg⁻¹ rat body weight + xylazine 15 mg kg⁻¹ rat body weight; ketamine 8 mg kg⁻¹ mouse body weight + xylazine 3 mg kg⁻¹ mouse body weight). The ICV cannulae aimed at the lateral ventricle were stereotaxically implanted in rats using the following coordinates: 1.3 mm posterior to bregma, 1.9 mm lateral to the midsagittal suture, and a depth of 3.5 mm; and in mice: 0.6 mm posterior to bregma, 1.2 mm lateral to the midsagittal suture and a depth of 2 mm (refs. [72,76]). Animals received vehicle (DMSO 100 mM) or bromocriptine mesylate (20, 40 or 80 µg per animal; Tocris). In other experiments, the orexin receptor 1 inhibitor (SB-334867; 4 µg per mouse, Tocris), orexin (10 µg per mouse, Bachem)[32,77], the specific PKA activator Sp-cAMPS (90 ng per rat dose; Tocris)[35,36], prolactin (1 or 10 µg per mouse) or cilostamide (10 µg per mouse, AlfaAesar)[39] were also administered ICV. For chronic experiments, a catheter tube connected from the brain infusion cannula to an osmotic minipump flow moderator (model 2002 for a 14-d period with rats and model 1007D for a 7-d period with mice; Alzet Osmotic Pumps). These pumps had a flow rate of 0.5 µl h⁻¹ during the days of treatment. The minipump was inserted in a subcutaneous pocket on the dorsal surface of the animal that we created using blunt dissection and the incision was closed with surgical sutures. After surgery, animals were kept warm until they fully recovered.

Peripheral treatments. For peripheral treatments, rats and mice received i.p. administered bromocriptine (40 µg per rat, mice 5 mg kg⁻¹). Mice received i.p. administered CNO (1 mg kg⁻¹, Sigma-Aldrich) and clozapine (1 mg kg⁻¹, Sigma-Aldrich)[27]. Pharmacological inactivation of β3-adrenoreceptor was performed by subcutaneous administration of the specific antagonist SR59230A (Tocris) at a dose of 3 mg kg⁻¹ (ref. [24]).

Stereotaxic microinjections in specific hypothalamic nuclei. Rats were placed in a stereotaxic frame (David Kopf Instruments) under ketamine-xylazine anaesthetics. Bromocriptine (40 µg per rat) and the specific PKA inhibitor H-89 (62 ng per rat; Sigma Chemicals) were injected stereotaxically with a 25-gauge needle (Hamilton) connected to a 1 µl syringe. We targeted the LHA/ZI and the VMH area[72]. The coordinates used to reach the LHA/ZI in rats were (anterior to the bregma (AP), −2.85 mm; lateral to the sagittal suture (L), ±2 mm; and ventral from the surface of the skull (DV), −8.1 mm) and to reach the VMH were AP, −2.85 mm; L, ±0.6 mm; DV, −10 mm. The coordinates used to reach the LHA/ZI in mice were AP, −1.3 mm; L, ±1.1 mm; DV, −5.2 mm, to reach the MBH were AP, −1.5 mm; L, ±0.2 mm; DV, −6 mm and to reach the DMH were AP, −1.9 mm; L, ±0.3 mm; DV, −5 mm). The incision was closed with sutures and acetylsalicylic acid (Bayer, Leverkusen, Germany) 150 mg kg⁻¹ was injected i.p. after surgery as a painkiller.

Stereotaxic microinjection of adenoviral expression vectors. Adenoviral vectors D2R knockdown (3.5 × 10¹⁰ plaque-forming units (p.f.u.) ml⁻¹) or the vector controls (3.5 × 10¹⁰ p.f.u. ml⁻¹) (ref. [78]) and adenoviral vectors containing the constitutively active form of S6K1 (4.77 × 10¹⁰ p.f.u. ml⁻¹) or null controls (1.8 × 10¹⁰ p.f.u. ml⁻¹) (ref. [43]) were used. To modify the expression of D2R specifically in vgat and vglut2 neurons, we injected Ad-hSyn-DIO-D2R-EGFP (1.0 × 10¹⁰ p.f.u. ml⁻¹), Ad-hSyn-DIO-shD2R-EGFP (1.0 × 10¹⁰ p.f.u. ml⁻¹) and

Fig. 6 | S6 mediates the effects of bromocriptine on BAT. a–i, rpS6 phosphorylated levels in the LHA/ZI after ICV injection of BC (40 µg) assessed by western blotting (n = 7) (**a**) and immunohistochemistry (n = 4) (**b**); 24-h specific injection of BC (40 µg) in the LHA/ZI (n = 7) (**c**); injection of Ad-GFP or Ad-shD2R in the LHA/ZI of rats treated with ICV BC (40 µg) (n = 6 GFP vehicle, n = 7 GFP BC, n = 7 D2R-KD vehicle and n = 7 D2R-KD BC) (**d**); 24-h ICV injection of BC (40 µg) in WT (n = 4) and OX knockout mice (n = 6)(**e**); injection of AAV-hSYN-DIO-hM3D (Gq)-mCherry and the ICV injection of SB-334867 (4 µg) (n = 4 vehicle, n = 4 CNO and n = 5 CNO + SB-334867) (**f**); ICV injection of OX (10 µg) and SB-334867 (4 µg) (n = 6) (**g**); LHA/ZI injection of the specific PKA inhibitor H-89 (62 ng) (n = 7) (**h**); and ICV injection of BC (40 µg) and the specific PKA activator Sp-cAMPS (90 ng) after 24 h (n = 6) (**i**). **j**, Total and rpS6 phosphorylated levels in the LHA/ZI 3 weeks after the viral infection (n = 7). **k–o**, Effect of the injection of adenoviral particles encoding for Null or S6K1 in the LHA/ZI of rats treated with ICV BC (40 µg) on body weight change (**k**), food intake (**l**) and infrared thermal images and quantification of BAT interscapular temperature (**m**) (n = 8 ad null vehicle, n = 9 ad null BC, n = 8 ad S6K1 vehicle and n = 9 ad S6K1 BC); histology of BAT lipid content and quantification of lipid droplet average area (**n**); and BAT UCP1 protein levels (**o**) (n = 7). Dividing lines indicate splicings within the same gel. α-tubulin and β-actin were used to normalize protein levels. Data are mean ± s.d. Statistical differences according to a two-tailed Student's t-test (**a,c,d**), a two-sided Mann–Whitney U-test (**b,e,h,j**), a Kruskal–Wallis followed by Dunn post hoc test for multiple comparison (**f,g,i**) or a one-way ANOVA followed by Bonferroni post hoc multiple comparison test (**k–o**).

Ad-hSyn-DIO-EGFP (1.0×10^{10} p.f.u. ml⁻¹) (Vector Builder) under cell-specific cre promoters. These viral vectors were injected in the hypothalamic nuclei as described in the previous section.

FACS sorting and quantitative RT-PCR analyses. Viral infection was confirmed using FACS. The tuberal region of the hypothalamus of Vgat-cre + Ad-EGFP LHA/ZI mice were microdissected and enzymatically dissociated using the Papain
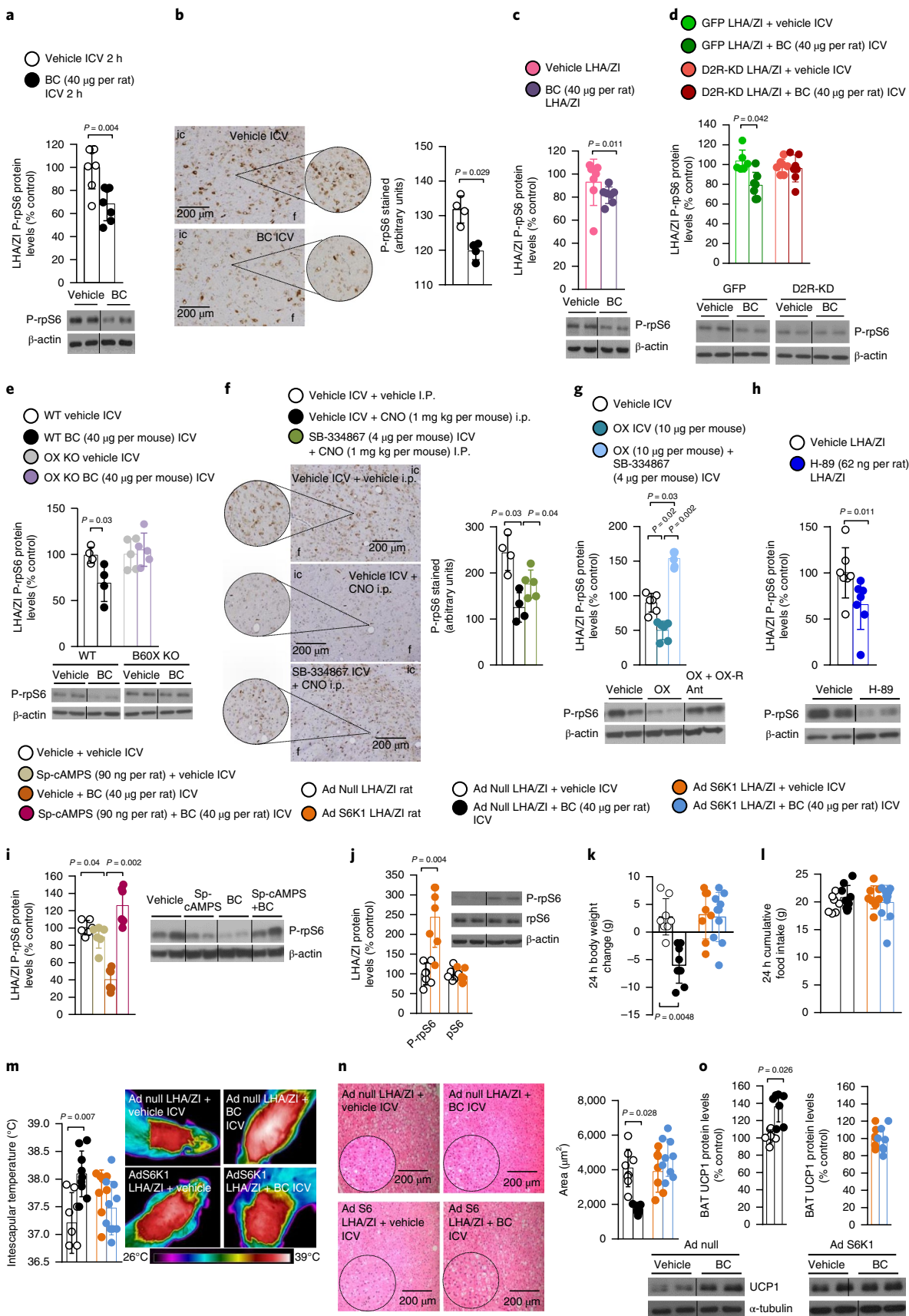
Table 1 | Clinical, anthropometric and metabolic characteristics of patients with hyperprolactinemia before and after one year of treatment with cabergoline

Condition or variable	Patients at diagnosis	Cabergoline treatment	P value
(n = 31)	Baseline	After 12 months	
Sex (m/f)	5/26	5/26	0.732
Age (years)	35 ± 10	36 ± 11	0.846
Body weight (kg)	67.5 ± 17.1	64.3 ± 14.2	0.045
BMI (kg m^{-2})	24.9 ± 5.4	23.8 ± 4.6	0.043
Prolactin (µg l^{-1})	99.5 ± 16.7	8.3 ± 9	<0.001
Glucose (mmol l^{-1})	5.8 ± 1.7	4.6 ± 1.5	0.038
Insulin (pmol l^{-1})	92 ± 48	79 ± 54	0.040
HOMA-IR	3.32 ± 2.15	2.26 ± 1.38	0.039
Triglycerides (mmol l^{-1})	2.0 ± 0.9	1.3 ± 0.5	0.008
Total cholesterol (mmol l^{-1})	5.0 ± 1.1	4.2 ± 0.6	0.041
LDL cholesterol (mmol l^{-1})	3.2 ± 1.0	2.1 ± 0.7	0.033
HDL cholesterol (mmol l^{-1})	1.1 ± 0.4	1.4 ± 0.5	0.075

Condition or variable	Patients at diagnosis	Cabergoline treatment		P value	
(n = 21)	Baseline	3 months	12 months	(a)	(b)
Sex (m/f)	3/18	3/18	3/18	0.806	
Age (years)	40 + 12	40 + 12	41 + 11	0.799	
Body weight (kg)	70.5 ± 10.6	64.6 ± 12.3	64.1 ± 15.0	0.044	0.045
BMI (kg m^{-2})	25.8 ± 5.1	24.2 ± 4.2	23.6 ± 5.3	0.042	0.043
WC (cm)	90 ± 11	84 ± 9	83 ± 10	0.047	0.046
Body fat (%)	34.7 ± 5.6	29.5 ± 4.2	28.9 ± 6.1	0.040	0.039
REE (kJ d^{-1})	5,997 ± 704	6,703 ± 800	6,532 ± 779	0.046	0.045
REE (kJ kg^{-1} d^{-1})	85.1 ± 9.2	104.2 ± 9.8	102.7 ± 8.6	0.041	0.040
REE (kJ kg^{-1} fat-free mass d^{-1})	90.0 ± 7.7	105.4 ± 5.6	101.9 ± 6.3	0.037	0.038
RQ (vCO$_2$/vO$_2$)	0.83 ± 0.06	0.84 ± 0.05	0.83 ± 0.08	0.621	0.665
Prolactin (µg l^{-1})	111.5 ± 12.7	9.3 ± 3.1	8.3 ± 5.0	<0.001	<0.001
Glucose (mmol l^{-1})	5.7 ± 0.8	4.1 ± 0.3	4.5 ± 0.5	0.042	0.04
Insulin (pmol l^{-1})	93 ± 56	71 ± 44	75 ± 52	0.037	0.036
HOMA-IR	3.53 ± 1.98	2.15 ± 1.59	2.43 ± 1.80	0.038	0.039
Triglycerides (mmol l^{-1})	2.1 ± 1.0	1.1 ± 0.3	1.3 ± 0.4	0.022	0.026
Total cholesterol (mmol l^{-1})	5.0 ± 0.9	4.7 ± 0.8	4.9 ± 1.0	0.278	0.301
LDL cholesterol (mmol l^{-1})	3.0 ± 1.1	2.5 ± 0.6	2.6 ± 0.8	0.293	0.352
HDL cholesterol (mmol l^{-1})	1.0 ± 0.6	1.2 ± 0.7	1.1 ± 0.5	0.348	0.386

WC, waist circumference; RQ, respiratory quotient; vCO$_2$/vO$_2$, dimensionless ratio between carbon dioxide production and oxygen consumption; comparison of baseline with (a) 3 months following cabergoline treatment initiation and (b) 12 months after cabergoline treatment start; according to a two-sided Student's t-tests between pre- and post-treatment values and Wilcoxon signed-rank test. Data are mean ± s.d.

Dissociation System to obtain single cell suspensions[79]. FACS was performed using an EPICS ALTRA Cell Sorter Cytometer device (BD Bioscience). The sort decision was based on measurements of EGFP fluorescence (excitation: 488 nm; 50 mW; detection: EGFP bandpass 530/30 nm, autofluorescence bandpass 695/40 nm) by comparing cell suspensions from non-infected brain sites (the cortex) and infected brain sites (the hypothalamus), as indicated in Fig. 4g. For each animal 150 to 400 EGFP-positive cells were sorted directly into 10 µl of extraction buffer: 0.1% Triton X-100 (Sigma-Aldrich) and 0.4 unit µl^{-1} RNaseOUT (Life Technologies). RNAs obtained from FACS-sorted EGFP-negative and positive cells were reversed transcribed using SuperScript III Reverse Transcriptase (Life Technologies) and a linear preamplification step was performed using the TaqMan PreAmp Master Mix Kit Protocol (P/N 4366128, Applied Biosystems). Real-time PCR quantification of VGat (*Slc32a1*-Mm00494138_m1), DR2 (*Drd2*-Mm00438545_m1) and VGlut2 (*Slc17a6*-Mm00499876_m1) was carried out on an Applied Biosystems 7900HT Fast Real-Time PCR system using exon-boundary-specific TaqMan Gene Expression Assays (Applied Biosystem). Control housekeeping genes were R18S (*r18S*-Mm03928990_g1) and Actin (*Actb*-Mm00607939_s1).

Designer receptors exclusively activated by designer drugs. The hM3Dq coding sequences were cloned into a mCherry vector upstream of the mCherry sequence to generate C-terminal mCherry fusion proteins (Addgene). The hM3Dq-mCherry coding sequence was amplified by PCR, and the amplicons and a cre-inducible AAV vector with a human *Synapsin 1* promoter was packaged in serotype 8: 7.53 × 10^{12} p.f.u. ml^{-1} genome copies per ml and was prepared and tittered at the Universidad Autónoma de Barcelona. Ketamine-xylazine anaesthesized male *D2-cre* mice[80] were placed in a stereotaxic frame (David Kopf Instruments). The CRE-dependent AAVs were injected bilaterally into the LHA/ZI of all mice. The viral particles (1 µl, 7.53 × 10^9 p.f.u. ml^{-1}) were infused over 15 min. Three weeks after the injection of the AAVs, mice received CNO (1 mg kg^{-1} of body weight) or vehicle i.p. injection.

Adenoviral injection in the BAT of mice. Adenoviral vectors for knocking down D2R (1.0 × 10^9 p.f.u. ml^{-1}) or the vector controls (1.0 × 10^9 p.f.u. ml^{-1}) were injected in a volume of 50 µl bilaterally into the BAT in mice under ketamine-xylazine [21].
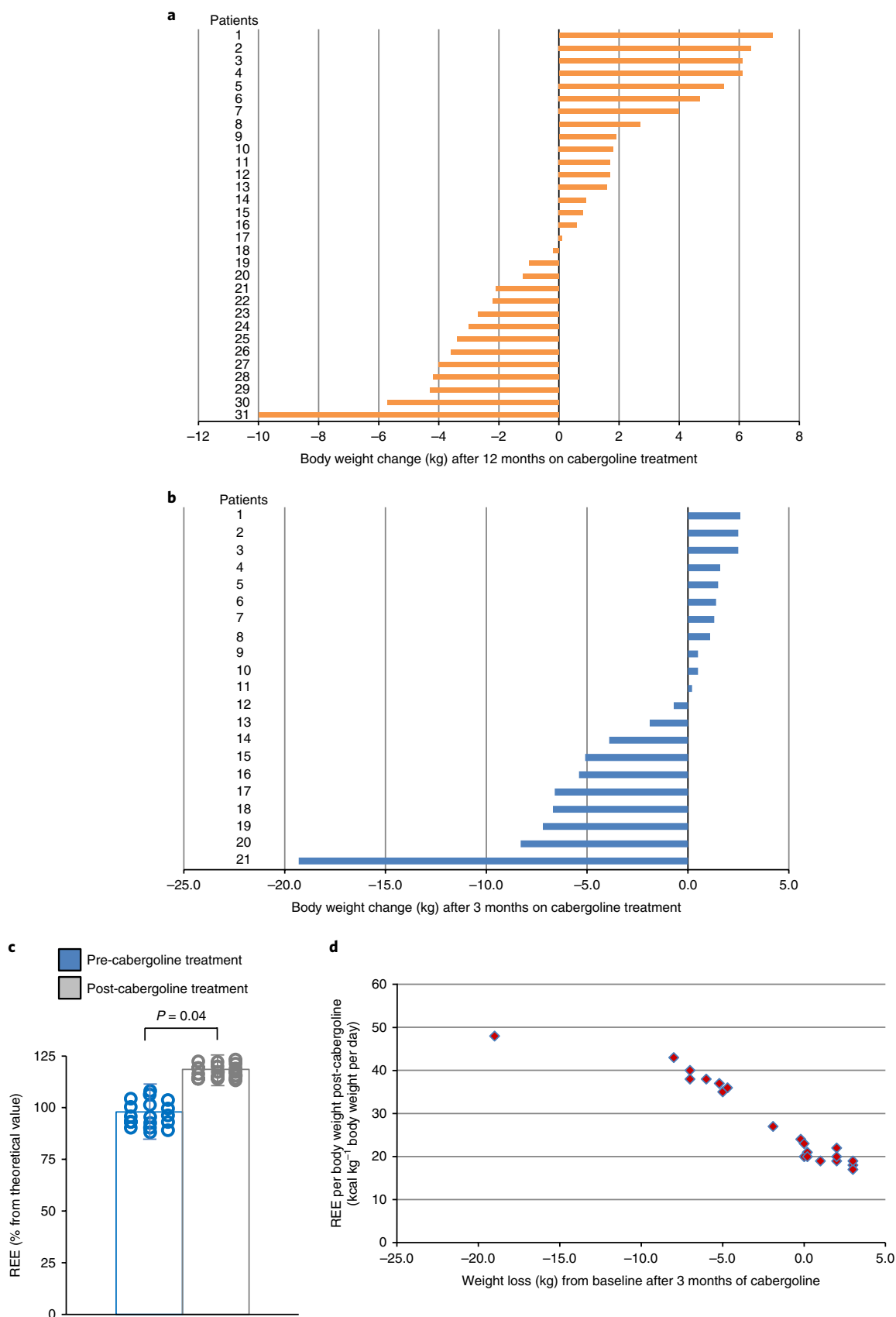
Fig. 7 | Cabergoline decreases body weight and increases REE in patients. a, Waterfall plot of the body weight changes experimented by each patient (1–31) of the retrospective study between baseline and following 0.5 mg twice weekly cabergoline treatment for 12 months. **b**, Waterfall plot of the body weight changes experimented by each patient (1–21) of the prospective study during the first 3 months of cabergoline treatment instauration with 0.5 mg cabergoline twice weekly. **c**, REE in patients before and after cabergoline treatment compared to the REE predicted from the Harris–Benedict equation. **d**, Correlation between REE and weight loss in patients treated with cabergoline.

PET imaging system. Whole-body micro PET-CT images were acquired with the Albira PET-CT Preclinical Imaging System (Bruker Biosping) and the experimental procedure with rats were performed in the same conditions. BAT area was delineated by using image tools implemented the AMIDE Software (http://amide.sourceforge.net/) to generate a three-dimensional spherical volume of interest with radius of 6 mm and centred on the BAT area. Mean standardized uptake values (SUV) were computed. The PET-CT analysis was performed in the Molecular Imaging Unit of the Department of Nuclear Medicine of University of Santiago de Compostela.

Dissection of brain areas. The brains were removed and immediately frozen and stored at −80 °C until further processing. Then, the brain was placed in a brain matrix with a ventral surface on top under a dissecting microscope. The LHA/ZI were removed from the whole hypothalamus by cutting between the rostral and caudal limits of the median eminence parallel to the base of the hypothalamus and 1 mm to each lateral side of the median eminence. The depth of each section isolated was around 1 mm thick in mice and 3 mm thick in rats brains[25,81].

Western blot analysis. Tissues were homogenized using a TissueLyser II (Qiagen) in cold RIPA buffer (containing 200 mMTris–HCl (pH 7.4), 130 mM NaCl, 10% (v/v) glycerol, 0.1% (v/v) SDS, 1% (v/v) Triton X-100, 10 mM MgCl$_2$) with antiproteases and antiphosphatases (Sigma-Aldrich). The tissue lysates were centrifuged for 30 min at 18,000g in a microfuge at 4 °C. BAT, muscle, cortex, VMH and LHA total protein lysates were subjected to sodium-dodecyl sulfate–polyacrylamide gels (SDS–PAGE), then electrotransferred onto a PVDF membrane and probed successively with the following antibodies: UCP1, FGF21, PRDM16, D2R, Myostatin (Abcam); PGC1α, JNK, MCH (Santa Cruz Biotechnology); pAKT (Ser473), AKT, phospho-S6 ribosomal protein, S6 ribosomal protein, phospho-SAPK/JNK (Thr183/Tyr185, phospho-CREB (Ser133) (Cell Signaling); GAPDH (Merck Millipore); mTOR, β-actin, α-tubulin (Sigma-Aldrich); Myogenin (DSHB); Orexin A (Bioss Antibodies); PDE3B (Invitrogen) after incubating the membranes with 5% bovine serum albumin blocking buffer. For the detection of proteins, we used horseradish-peroxidase-conjugated secondary antibodies (Dako Denmark). Specific antigen–antibody binding was visualized using a chemiluminescence method according to the manufacturer´s instructions (Pierce ECL Western Blotting Substrate, Thermo Scientific). Values were expressed in relation to β-actin or GAPDH (for cortex, VMH and LHA) and α-tubulin (for muscle and BAT) protein levels. For details related to antibodies and dilutions please see Reporting Summary. Uncropped images of all immunoblots are provided in Supplementary Fig. 11.

Blood determinations in rodents. The quantitative determination of mouse or rat prolactin concentrations in plasma was determined by enzyme-linked immunosorbent assays using reagents kits and methods provided by Mybiosurce (catalogue no. MBS 580033).

Histomorphology. BAT samples were fixed for 24 h in 10% formalin buffer and then were dehydrated and embedded in paraffin by a standard procedure. Sections of 3 μm were made in a microtome and stained with a standard hematoxilin and eosin alcoholic (BioOptica) procedure following manufacturer instructions[24]. Sections were observed and photographed using a Provis AX70 microscope (Olympus). BAT quantification was analysed using Image-J software (National Institutes of Health).

Immunohistochemistry and immunofluorescence. The detection of UCP1 in BAT was performed using anti-UCP1 (1:500; Abcam) with an anti-rabbit antibody conjugated with Alexa 488 (1:200; Molecular Probes)[24]. Images were observed and photographed using a Provis AX70 microscope (Olympus) and were quantified with Framework for Image Dataset Analysis software.

Animal brains were fixed by perfusion after they were inmersion-fixed in formol-calcium for 24 h. They were then dehydrated and embedded in paraffin and were cut and mounted using a thick section of 3 μm (Vibratome Series 1000, The Vibratome Company)[82]. Sections were incubated overnight at 4 °C with anti-phospho-S6 ribosomal (Cell Signaling) diluted 1:200 in EnVision Flex Antibody diluent (DAKO). After washes, sections were incubated with LSAB-DAKO secondary for 30 min. In addition, brains were processed and immunohistochemistry assays were performed to visualize protein levels of c-FOS (Santa Cruz) at a dilution of 1:500 (ref. [72]). Images were observed and photographed using a Provis AX70 microscope (Olympus). Cellular counting was performed in the brain using Image-J software.

To test specific nuclei injection, we used immunofluorescence. To visualize green positive signals, sections were incubated with rabbit antibody against GFP (1:200; Abcam) and we used a goat anti-rabbit Alexa 488 (1:200; Molecular Probes).

Detection of mCherry was performed with an immunofluorescence procedure, using a rabbit anti-cherry (1:200; Abcam). Detection was done with an anti-rabbit antibody conjugated with Alexa 488 (1:200; Molecular Probes).

Tissue preparation, immunofluorescence and quantification were performed as described[26]. The following primary antibodies were used: mouse anti-HA (1:1,000, Covance, MMS-101R), chicken anti-GFP (1:500, Life technologies (A10262), rabbit anti-VGlut2 (1:500, Synaptic Systems, 135402), anti-VGat (1:1,000, Synaptic Systems, 131013), anti-orexin-A (1:500, Millipore AB3098) and anti-MCH (1:500, Sigma, M8440). LHA and ZI sections were identified using a mouse brain atlas and sections between −1.34 and −1.70 mm from bregma were analysed.

In situ hybridization. Coronal hypothalamic sections (16 μm) were cut on a cryostat and immediately stored at −80 °C until hybridization. For MCH and prepro-OX mRNA detection, we used specific antisense oligodeoxynucleotides (Supplementary Table 1). These probes were 3′-end labelled with [α-35S]deoxy-ATP using terminal deoxynucleotidyl transferase. The frozen sections were fixed with 4% paraformaldehyde in 0.1 m phosphate buffer (pH 7.4) at room temperature for 30 min. They were then dehydrated using 70%, 80%, 90%, 95% and absolute ethanol (5 min each). The hybridization was carried out overnight at 37 °C in a moist chamber. The hybridization solution contained 5 × 10⁵ (prepro-OX) or 1 × 10⁶ c.p.m. (MCH) per slide of the labelled probe, 4 × standard saline citrate (SSC), 50% deionized formamide, 1 × Denhardt's solution, 10% dextran sulfate and 10 μg ml⁻¹ sheared, single-stranded salmon sperm DNA. Afterwards, the hybridization sections were sequentially washed in 1 × SSC at room temperature, four times in 1 × SSC at 42 °C (30 min per wash) and once in 1 × SSC at room temperature (1 h), and then rinsed in water and ethanol. Finally, the sections were air-dried and exposed to Hyperfilm β-Max (Amersham International) at room temperature for 4–6 d (ref. [83]). Images were quantified using ImageJ software.

Patient selection. First, we conducted a retrospective chart review of patients with hyperprolactinemia who attended the Endocrinology Department of the University Clinic of Navarra between January 2007 and December 2013. All patients were of Caucasian origin. Pregnant and lactating women were excluded. Patients with hyperprolactinemia secondary to drugs (including neuroleptics, antidepressants, opiates and gastrointestinal prokinetics) or mixed-secreting tumours or those already receiving dopamine agonists at the first visit to our hospital, as well as those not completing a 12-month follow-up period, were excluded from the analysis. Furthermore, patients with multiple pituitary hormone deficiencies and/or the presence of other concomitant causes of overt hypogonadism were excluded to avoid the potential effect of hormonal replacement therapy on body weight control and metabolic changes. In this respect, patients with previously known treatment with hypoglycaemic agents to control glucose metabolism abnormalities or antiobesity drugs for body weight loss were also excluded. After all the exclusions, 31 patients with newly diagnosed prolactinoma comprised the study sample of the retrospective analysis (26 females and 5 males with an age range between 21 and 61 years). All patients underwent a detailed anamnesis, physical exploration and metabolic evaluation (Reporting Summary). The diagnosis was based on signs and symptoms of hyperprolactinemia, high serum prolactin concentrations and magnetic resonance imaging demonstrating a pituitary tumour[84]. After the diagnosis patients received cabergoline, a potent long-acting dopamine agonist that is more effective and better tolerated than bromocriptine[85]. Cabergoline was administered orally at a starting dose of 0.25 mg once weekly at bedtime for the first week, twice weekly during the second week and escalating until administration of 0.5 mg twice weekly at bedtime. Prolactin normalization was achieved with this treatment protocol in all patients.

To examine in more detail the potential impact of dopamine agonism on body weight, body composition, REE and metabolic changes a prospective study was carried out in patients with hyperprolactinemia seen at the same Endocrinology Department of the University Clinic of Navarra between January 2014 and May 2017 (Reporting Summary). The same inclusion and exclusion criteria and treatment protocol as for the retrospective study were applied. In this case, however, body composition, as well as REE determinations, were performed at baseline when the diagnosis was established as well as at the follow-up visits at 3, 6 and 12 months after treatment instauration with cabergoline. In the prospective study, 22 patients of Caucasian origin with newly diagnosed prolactinoma were enroled (19 females and 3 males with an age range between 25 and 63 years). All patients were non-smokers and did not show signs of infection. Both clinical studies were approved, from an ethical and scientific standpoint, by the Hospital's Ethical Committee and were conducted in accordance with the principles of the Declaration of Helsinki with patients giving their informed consent for participation.

Anthropometry. Body weight was measured with a digital scale to the nearest 0.1 kg, while height was measured to the nearest 0.1 cm with a Holtain stadiometer (Holtain Ltd.) to calculate the BMI. Waist circumference was determined at the midpoint between the iliac crest and the rib cage on the midaxillary line. Body fat was estimated by air-displacement-plethysmography (Bod-Pod, Life Measurements)[86].

Indirect calorimetry. In the prospective study the REE and respiratory quotient were determined by indirect calorimetry after a 12-h overnight fast using an open-air-circuit ventilated canopy measurement system (Vmax29, SensorMedics Corporation) at baseline and at follow-up visits after treatment start adjusting also for body composition[87].

Blood determinations in humans. Plasma samples were obtained by venipuncture after an overnight fast. Glucose was analyzed on the basis of enzymatic spectrophotometric reactions by an automated analyzer (Hitachi Modular P800, Roche). Insulin was measured by means of an enzyme-amplified chemiluminescence assay (IMMULITE, Diagnostic Products Corp.). The intra- and interassay coefficients of variation (CV) were 4.2% and 5.7%, respectively. Insulin resistance was calculated using the HOMA-IR index. Circulating prolactin

concentrations were determined by a microparticle chemiluminescent assay (Prolactin II, Elecsys, Cobas E, Roche Diagnostics GmbH.) with a normal range of $1-27\,\mu g\,l^{-1}$ for women and of $1-20\,\mu g\,l^{-1}$ for men together with intra- and interassay CV of 2.3 and 5.9%, respectively. Triglycerides, total cholesterol, HDL-cholesterol and LDL-cholesterol levels were calculated as previously described[88].

Statistical analysis. Results are given as mean ± s.d. Samples or animals were excluded if values were outside ± 2-fold s.d.[89] or if an objective experimental failure was observed; studies were not blinded to investigators or formally randomized. The number of animals used in each study is listed in the figure legends. To test if the populations follows a Gaussian distribution, a normality test was performed (Kolgomorov–Smirnov test for n between 5 and 7; Shapiro–Wilk test for $n \geq 7$) (ref. [90]). For normal distributions, a parametric test was used; for two population comparisons, an unpaired t-test (two-tailed for treatment and phenotyping experiment, one-tailed otherwise) were used as indicated in figure legends[91–93]; for multiple comparison test, a one-way analysis of variance (ANOVA) followed by Bonferroni post hoc multiple comparison test was performed[94]. For non-Gaussian distributions, the following were used: Mann–Whitney tests were used for two comparison tests[95] and Kruskal–Wallis followed by Dunn post hoc test for multiple comparison[96,97]. Data analysis was performed using GraphPad Prism Software v.5.0 (GraphPad). The correlation between locomotor activity and energy expenditure was analysed by Pearson's correlation (normally distributed data) or Spearman's rank correlation (non-normally distributed data) coefficients (r). Data analysis was performed using the SPSS v.20.0 software statistical package (SPSS) (Reporting Summary).

In patients, comparison of changes at baseline and after treatment administration at different time points was carried out by two-tailed paired Student's t-tests between pre- and post-treatment values and Wilcoxon signed-rank test as appropriate. The calculations were performed using the SPSS/Windows v.15.0 statistical package (SPSS) (Reporting Summary). A P value <0.05 was considered statistically significant.

Reporting Summary. Further information on research design is available in the Nature Research Reporting Summary linked to this article.

Data availability
The data that support the findings of this study are available from the corresponding author upon request.

References
1. Palmiter, R. D. Is dopamine a physiologically relevant mediator of feeding behavior? *Trends Neurosci.* **30**, 375–381 (2007).
2. Mirmohammadsadeghi, Z., Shareghi Brojeni, M., Haghparast, A. & Eliassi, A. Role of paraventricular hypothalamic dopaminergic D1 receptors in food intake regulation of food-deprived rats. *Eur. J. Pharmacol.* **818**, 43–49 (2018).
3. Zhu, X., Ottenheimer, D. & DiLeone, R. J. Activity of D1/2 receptor expressing neurons in the nucleus accumbens regulates running, locomotion, and food intake. *Front. Behav. Neurosci.* **10**, 66 (2016).
4. Land, B. B. et al. Medial prefrontal D1 dopamine neurons control food intake. *Nat. Neurosci.* **17**, 248–253 (2014).
5. Fetissov, S. O., Meguid, M. M., Sato, T. & Zhang, L. H. Expression of dopaminergic receptors in the hypothalamus of lean and obese zucker rats and food intake. *Am. J. Physiol. Regulatory, Integr. Comp. Physiol.* **283**, R905–R910 (2002).
6. Johnson, P. M. & Kenny, P. J. Dopamine D2 receptors in addiction-like reward dysfunction and compulsive eating in obese rats. *Nat. Neurosci.* **13**, 635–641 (2010).
7. Volkow, N. D., Wang, G. J. & Baler, R. D. Reward, dopamine and the control of food intake: implications for obesity. *Trends Cogn. Sci.* **15**, 37–46 (2011).
8. Wang, G. J., Volkow, N. D. & Fowler, J. S. The role of dopamine in motivation for food in humans: implications for obesity. *Expert Opin. Ther. Targets* **6**, 601–609 (2002).
9. Holt, R. I., Barnett, A. H. & Bailey, C. J. Bromocriptine: old drug, new formulation and new indication. *Diabetes, Obes. Metab.* **12**, 1048–1057 (2010).
10. Cincotta, A. H. & Meier, A. H. Bromocriptine (Ergoset) reduces body weight and improves glucose tolerance in obese subjects. *Diabetes Care* **19**, 667–670 (1996).
11. Pijl, H. et al. Bromocriptine: a novel approach to the treatment of type 2 diabetes. *Diabetes Care* **23**, 1154–1161 (2000).
12. Gaziano, J. M. et al. Randomized clinical trial of quick-release bromocriptine among patients with type 2 diabetes on overall safety and cardiovascular outcomes. *Diabetes Care* **33**, 1503–1508 (2010).
13. Wang, G. J. et al. Brain dopamine and obesity. *Lancet* **357**, 354–357 (2001).
14. Bray, G. A., Fruhbeck, G., Ryan, D. H. & Wilding, J. P. Management of obesity. *Lancet* **387**, 1947–1956 (2016).
15. Henderson, D. C., Vincenzi, B., Andrea, N. V., Ulloa, M. & Copeland, P. M. Pathophysiological mechanisms of increased cardiometabolic risk in people with schizophrenia and other severe mental illnesses. *Lancet Psychiatry* **2**, 452–464 (2015).
16. Noble, E. P. et al. D2 dopamine receptor gene and obesity. *Int. J. Eat. Disord.* **15**, 205–217 (1994).
17. Sun, X., Luquet, S. & Small, D. M. DRD2: Bridging the genome and ingestive behavior. *Trends Cogn. Sci.* **21**, 372–384 (2017).
18. Meier, A. H., Cincotta, A. H. & Lovell, W. C. Timed bromocriptine administration reduces body fat stores in obese subjects and hyperglycemia in type II diabetics. *Experientia* **48**, 248–253 (1992).
19. Gibson, C. D., Karmally, W., McMahon, D. J., Wardlaw, S. L. & Korner, J. Randomized pilot study of cabergoline, a dopamine receptor agonist: effects on body weight and glucose tolerance in obese adults. *Diabetes, Obes. Metab.* **14**, 335–340 (2012).
20. Liu, X. et al. The mechanism and pathways of dopamine and dopamine agonists in prolactinomas. *Front. Endocrinol.* **9**, 768 (2018).
21. Al-Massadi, O. et al. Pharmacological and genetic manipulation of p53 in brown fat at adult but not embryonic stages regulates thermogenesis and body weight in male mice. *Endocrinology* **157**, 2735–2749 (2016).
22. Fruhbeck, G., Mendez-Gimenez, L., Fernandez-Formoso, J. A., Fernandez, S. & Rodriguez, A. Regulation of adipocyte lipolysis. *Nutr. Res. Rev.* **27**, 63–93 (2014).
23. Hankir, M. K., Cowley, M. A. & Fenske, W. K. A BAT-centric approach to the treatment of diabetes: Turn on the brain. *Cell Metab.* **24**, 31–40 (2016).
24. Folgueira, C. et al. Uroguanylin action in the brain reduces weight gain in obese mice via different efferent autonomic pathways. *Diabetes* **65**, 421–432 (2016).
25. Martinez-Sanchez, N. et al. Hypothalamic AMPK-ER stress-JNK1 axis mediates the central actions of thyroid hormones on energy balance. *Cell Metab.* **26**, 212–229 e212 (2017).
26. Weiner, D. M. et al. D1 and D2 dopamine receptor mRNA in rat brain. *Proc. Natl Acad. Sci. USA* **88**, 1859–1863 (1991).
27. Gomez, J. L. et al. Chemogenetics revealed: DREADD occupancy and activation via converted clozapine. *Science* **357**, 503–507 (2017).
28. Stagkourakis, S., Kim, H., Lyons, D. J. & Broberger, C. Dopamine autoreceptor regulation of a hypothalamic dopaminergic network. *Cell Rep.* **15**, 735–747 (2016).
29. Puighermanal, E. et al. drd2-cre:ribotag mouse line unravels the possible diversity of dopamine d2 receptor-expressing cells of the dorsal mouse hippocampus. *Hippocampus* **25**, 858–875 (2015).
30. Segal-Lieberman, G. et al. Melanin-concentrating hormone is a critical mediator of the leptin-deficient phenotype. *Proc. Natl Acad. Sci. USA* **100**, 10085–10090 (2003).
31. Tupone, D., Madden, C. J., Cano, G. & Morrison, S. F. An orexinergic projection from perifornical hypothalamus to raphe pallidus increases rat brown adipose tissue thermogenesis. *J. Neurosci.* **31**, 15944–15955 (2011).
32. Martins, L. et al. A functional link between AMPK and orexin mediates the effect of BMP8B on energy balance. *Cell Rep.* **16**, 2231–2242 (2016).
33. Yamaguchi, T. et al. Role of PKA signaling in D2 receptor-expressing neurons in the core of the nucleus accumbens in aversive learning. *Proc. Natl Acad. Sci. USA* **112**, 11383–11388 (2015).
34. Bonito-Oliva, A. et al. Haloperidol promotes mTORC1-dependent phosphorylation of ribosomal protein S6 via dopamine- and cAMP-regulated phosphoprotein of 32 kDa and inhibition of protein phosphatase-1. *Neuropharmacology* **72**, 197–203 (2013).
35. Mighiu, P. I. et al. Hypothalamic glucagon signaling inhibits hepatic glucose production. *Nat. Med.* **19**, 766–772 (2013).
36. Quinones, M. et al. Hypothalamic CaMKKbeta mediates glucagon anorectic effect and its diet-induced resistance. *Mol. Metab.* **4**, 961–970 (2015).
37. Meacci, E. et al. Molecular cloning and expression of human myocardial cGMP-inhibited cAMP phosphodiesterase. *Proc. Natl Acad. Sci. USA* **89**, 3721–3725 (1992).
38. Zhao, A. Z., Huan, J. N., Gupta, S., Pal, R. & Sahu, A. A phosphatidylinositol 3-kinase phosphodiesterase 3B-cyclic AMP pathway in hypothalamic action of leptin on feeding. *Nat. Neurosci.* **5**, 727–728 (2002).
39. Sahu, M., Anamthathmakula, P. & Sahu, A. Hypothalamic phosphodiesterase 3B pathway mediates anorectic and body weight-reducing effects of insulin in male mice. *Neuroendocrinology* **104**, 145–156 (2017).
40. Sahu, M., Anamthathmakula, P. & Sahu, A. Phosphodiesterase-3B-cAMP pathway of leptin signalling in the hypothalamus is impaired during the development of diet-induced obesity in FVB/N mice. *J. Neuroendocrinol.* **27**, 293–302 (2015).
41. Moore, C. E., Xie, J., Gomez, E. & Herbert, T. P. Identification of cAMP-dependent kinase as a third in vivo ribosomal protein S6 kinase in pancreatic beta-cells. *J. Mol. Biol.* **389**, 480–494 (2009).
42. Valjent, E. et al. Haloperidol regulates the state of phosphorylation of ribosomal protein S6 via activation of PKA and phosphorylation of DARPP-32. *Neuropsychopharmacol.* **36**, 2561–2570 (2011).

43. Blouet, C., Ono, H. & Schwartz, G. J. Mediobasal hypothalamic p70 S6 kinase 1 modulates the control of energy homeostasis. *Cell Metab.* **8**, 459–467 (2008).

44. Richard, D. Cognitive and autonomic determinants of energy homeostasis in obesity. *Nat. Rev. Endocrinol.* **11**, 489–501 (2015).

45. Meguid, M. M., Yang, Z. J. & Montante, A. Lateral hypothalamic dopaminergic neural activity in response to total parenteral nutrition. *Surgery* **114**, 400–405 (1993). discussion 405-406.

46. Meguid, M. M., Yang, Z. J. & Koseki, M. Eating induced rise in LHA-dopamine correlates with meal size in normal and bulbectomized rats. *Brain Res. Bull.* **36**, 487–490 (1995).

47. Yang, Z. J., Koseki, M., Meguid, M. M. & Laviano, A. Eating-related increase of dopamine concentration in the LHA with oronasal stimulation. *Am. J. Physiol.* **270**, R315–R318 (1996).

48. Najam, N. Involvement of dopaminergic systems in the ventromedial hypothalamic hyperphagia. *Brain Res. Bull.* **21**, 571–574 (1988).

49. Baptista, T., Parada, M. & Hernandez, L. Long term administration of some antipsychotic drugs increases body weight and feeding in rats. Are D2 dopamine receptors involved? *Pharmacol. Biochem. Behav.* **27**, 399–405 (1987).

50. Meguid, M. M., Yang, Z. J. & Laviano, A. Meal size and number: relationship to dopamine levels in the ventromedial hypothalamic nucleus. *Am. J. Physiol.* **272**, R1925–R1930 (1997).

51. Meguid, M. M. et al. Hypothalamic dopamine and serotonin in the regulation of food intake. *Nutrition* **16**, 843–857 (2000).

52. Zhang, X. & van den Pol, A. N. Hypothalamic arcuate nucleus tyrosine hydroxylase neurons play orexigenic role in energy homeostasis. *Nat. Neurosci.* **19**, 1341–1347 (2016).

53. Labouesse, M. A. et al. Striatal dopamine 2 receptor upregulation during development predisposes to diet-induced obesity by reducing energy output in mice. *Proc. Natl Acad. Sci. USA* **115**, 10493–10498 (2018).

54. Carlin, J., Hill-Smith, T. E., Lucki, I. & Reyes, T. M. Reversal of dopamine system dysfunction in response to high-fat diet. *Obesity* **21**, 2513–2521 (2013).

55. Friend, D. M. et al. Basal ganglia dysfunction contributes to physical inactivity in obesity. *Cell Metab.* **25**, 312–321 (2017).

56. Lopez, M., Nogueiras, R., Tena-Sempere, M. & Dieguez, C. Hypothalamic AMPK: a canonical regulator of whole-body energy balance. *Nat. Rev. Endocrinol.* **12**, 421–432 (2016).

57. Kohlie, R. et al. Dopamine directly increases mitochondrial mass and thermogenesis in brown adipocytes. *J. Mol. Endocrinol.* **58**, 57–66 (2017).

58. Burt, J., Alberto, C. O., Parsons, M. P. & Hirasawa, M. Local network regulation of orexin neurons in the lateral hypothalamus. *Am. J. Physiol. Regulatory, Integr. Comp. Physiol.* **301**, R572–R580 (2011).

59. Bubser, M. et al. Dopaminergic regulation of orexin neurons. *Eur. J. Neurosci.* **21**, 2993–3001 (2005).

60. Yasuda, T. et al. Dual regulatory effects of orexins on sympathetic nerve activity innervating brown adipose tissue in rats. *Endocrinology* **146**, 2744–2748 (2005).

61. Sellayah, D., Bharaj, P. & Sikder, D. Orexin is required for brown adipose tissue development, differentiation, and function. *Cell Metab.* **14**, 478–490 (2011).

62. Stoof, J. C. & Kebabian, J. W. Opposing roles for D-1 and D-2 dopamine receptors in efflux of cyclic AMP from rat neostriatum. *Nature* **294**, 366–368 (1981).

63. Yang, L. & McKnight, G. S. Hypothalamic PKA regulates leptin sensitivity and adiposity. *Nat. Commun.* **6**, 8237 (2015).

64. Cummings, D. E. et al. Genetically lean mice result from targeted disruption of the RII beta subunit of protein kinase A. *Nature* **382**, 622–626 (1996).

65. Zheng, R. et al. Deficiency of the RIIbeta subunit of PKA affects locomotor activity and energy homeostasis in distinct neuronal populations. *Proc. Natl Acad. Sci. USA* **110**, E1631–E1640 (2013).

66. Inancli, S. S. et al. Effect of cabergoline on insulin sensitivity, inflammation, and carotid intima media thickness in patients with prolactinoma. *Endocrine* **44**, 193–199 (2013).

67. Pala, N. A., Laway, B. A., Misgar, R. A. & Dar, R. A. Metabolic abnormalities in patients with prolactinoma: response to treatment with cabergoline. *Diabetol. Metab. Syndr.* **7**, 99 (2015).

68. Lamos, E. M., Levitt, D. L. & Munir, K. M. A review of dopamine agonist therapy in type 2 diabetes and effects on cardio-metabolic parameters. *Prim. Care Diabetes* **10**, 60–65 (2016).

69. Nogueiras, R. et al. Direct control of peripheral lipid deposition by CNS GLP-1 receptor signaling is mediated by the sympathetic nervous system and blunted in diet-induced obesity. *J. Neurosci.* **29**, 5916–5925 (2009).

70. Nogueiras, R. et al. The central melanocortin system directly controls peripheral lipid metabolism. *J. Clin. Investig.* **117**, 3475–3488 (2007).

71. Gangarossa, G. et al. Characterization of dopamine D1 and D2 receptor-expressing neurons in the mouse hippocampus. *Hippocampus* **22**, 2199–2207 (2012).

72. Beiroa, D. et al. GLP-1 agonism stimulates brown adipose tissue thermogenesis and browning through hypothalamic AMPK. *Diabetes* **63**, 3346–3358 (2014).

73. Contreras, C. et al. Central ceramide-induced hypothalamic lipotoxicity and ER stress regulate energy balance. *Cell Rep.* **9**, 366–377 (2014).

74. Czyzyk, T. A. et al. Mice lacking delta-opioid receptors resist the development of diet-induced obesity. *FASEB J.* **26**, 3483–3492 (2012).

75. Alvarez-Crespo, M. et al. Essential role of UCP1 modulating the central effects of thyroid hormones on energy balance. *Mol. Metab.* **5**, 271–282 (2016).

76. Imbernon, M. et al. Hypothalamic kappa opioid receptor mediates both diet-induced and melanin concentrating hormone-induced liver damage through inflammation and endoplasmic reticulum stress. *Hepatology* **64**, 1086–1104 (2016).

77. Alvarez-Crespo, M. et al. The orexigenic effect of orexin-A revisited: dependence of an intact growth hormone axis. *Endocrinology* **154**, 3589–3598 (2013).

78. de Jong, J. W. et al. Reducing ventral tegmental dopamine D2 receptor expression selectively boosts incentive motivation. *Neuropsychopharmacol.* **40**, 2085–2095 (2015).

79. Messina, A. et al. A microRNA switch regulates the rise in hypothalamic GnRH production before puberty. *Nat. Neurosci.* **19**, 835–844 (2016).

80. Konner, A. C. et al. Insulin action in AgRP-expressing neurons is required for suppression of hepatic glucose production. *Cell Metab.* **5**, 438–449 (2007).

81. Lopez, M. et al. Hypothalamic AMPK and fatty acid metabolism mediate thyroid regulation of energy balance. *Nat. Med.* **16**, 1001–1008 (2010).

82. Imbernon, M. et al. Central melanin-concentrating hormone influences liver and adipose metabolism via specific hypothalamic nuclei and efferent autonomic/JNK1 pathways. *Gastroenterology* **144**, 636–649 e636 (2013).

83. Seoane, L. M. et al. Agouti-related peptide, neuropeptide Y, and somatostatin-producing neurons are targets for ghrelin actions in the rat hypothalamus. *Endocrinology* **144**, 544–551 (2003).

84. Melmed, S. et al. Diagnosis and treatment of hyperprolactinemia: an Endocrine Society clinical practice guideline. *J. Clin. Endocrinol. Metab.* **96**, 273–288 (2011).

85. Webster, J. et al. A comparison of cabergoline and bromocriptine in the treatment of hyperprolactinemic amenorrhea. Cabergoline comparative study group. *N. Engl. J. Med.* **331**, 904–909 (1994).

86. Gómez-Ambrosi, J. et al. Body adiposity and type 2 diabetes: increased risk with a high body fat percentage even having a normal BMI. *Obesity* **19**, 1439–1444 (2011).

87. Sabater, M. et al. Circulating pigment epithelium-derived factor levels are associated with insulin resistance and decrease after weight loss. *J. Clin. Endocrinol. Metab.* **95**, 4720–4728 (2010).

88. Gómez-Ambrosi, J. et al. Involvement of leptin in the association between percentage of body fat and cardiovascular risk factors. *Clin. Biochem.* **35**, 315–320 (2002).

89. Miller, J. Reaction time analysis with outlier exclusion: bias varies with sample size. *Q. J. Exp. Psychol. A, Hum. Exp. Psychol.* **43**, 907–912 (1991).

90. Razali, N. M. & Wah, Y. B. Power comparisons of shapiro-wilk, kolmogorov-smirnov, lilliefors and anderson-darling tests. *J. Stat. Modeling Analytics* **2**, 21–33 (2011).

91. Student. The probable error of a mean. *Biometrika* **6**, 1–25 (1908).

92. Fay, D. S. & Gerow, K. A biologist's guide to statistical thinking and analysis. *WormBook: the Online Review of C. elegans Biology* (2013); https://doi.org/10.1895/wormbook.1891.1159.1891

93. Charan, J. & Biswas, T. How to calculate sample size for different study designs in medical research? *Indian J. Psychological Med.* **35**, 121–126 (2013).

94. Kao, L. S. & Green, C. E. Analysis of variance: Is there a difference in means and what does it mean? *J. Surgical Res.* **144**, 158–170 (2008).

95. Bridge, P. D. & Sawilowsky, S. S. Increasing physicians' awareness of the impact of statistics on research outcomes. *J. Clin. Epidemiol.* **52**, 229–235 (1999).

96. Dunn, O. J. Multiple comparisons using rank sums. *Technometrics* **6**, 241–252 (1964).

97. Campbell, G. & Skillings, J. H. Nonparametric stepwise multiple comparison procedures. *J. Am. Stat. Assoc.* **80**, 998–1003 (1985).

Acknowledgements

Author contributions

C.F., D.B., B.P., M.D., E.P., M.F.-F., S.B.-F., R.G., R.H.-B., C.C., A.S., P.S.-C., N.G.-L., P.A., D.G., M.F., A.R.-R., I.K. and Z.L. carried out the experiments. R.A., C.B., J.L.L.-B. and F.J. generated viral vectors and animal models. J.S. and G.F. performed the assays in patients. C.F., V.P., C.D., M.L., E.V., L.M.S. and R.N. designed and planned the study. All authors contributed to the preparation of the manuscript.

Competing interests

The authors declare no competing interests.

Additional information

Supplementary information is available for this paper at https://doi.org/10.1038/s42255-019-0099-7.

Reprints and permissions information is available at www.nature.com/reprints.

Correspondence and requests for materials should be addressed to L.M.S. or R.N.

Peer review information: Primary Handling Editor: Elena Bellafante

Publisher's note: Springer Nature remains neutral with regard to jurisdictional claims in published maps and institutional affiliations.

nature research

Corresponding author(s): Rubén Nogueiras

Last updated by author(s): Jul 3, 2019

Reporting Summary

Nature Research wishes to improve the reproducibility of the work that we publish. This form provides structure for consistency and transparency in reporting. For further information on Nature Research policies, see Authors & Referees and the Editorial Policy Checklist.

Statistics

For all statistical analyses, confirm that the following items are present in the figure legend, table legend, main text, or Methods section.

n/a	Confirmed	
☐	☒	The exact sample size (*n*) for each experimental group/condition, given as a discrete number and unit of measurement
☐	☒	A statement on whether measurements were taken from distinct samples or whether the same sample was measured repeatedly
☐	☒	The statistical test(s) used AND whether they are one- or two-sided *Only common tests should be described solely by name; describe more complex techniques in the Methods section.*
☐	☒	A description of all covariates tested
☐	☒	A description of any assumptions or corrections, such as tests of normality and adjustment for multiple comparisons
☐	☒	A full description of the statistical parameters including central tendency (e.g. means) or other basic estimates (e.g. regression coefficient) AND variation (e.g. standard deviation) or associated estimates of uncertainty (e.g. confidence intervals)
☐	☒	For null hypothesis testing, the test statistic (e.g. *F*, *t*, *r*) with confidence intervals, effect sizes, degrees of freedom and *P* value noted *Give P values as exact values whenever suitable.*
☒	☐	For Bayesian analysis, information on the choice of priors and Markov chain Monte Carlo settings
☒	☐	For hierarchical and complex designs, identification of the appropriate level for tests and full reporting of outcomes
☒	☐	Estimates of effect sizes (e.g. Cohen's *d*, Pearson's *r*), indicating how they were calculated

Our web collection on statistics for biologists contains articles on many of the points above.

Software and code

Policy information about availability of computer code

Data collection	Microsoft Excel 2010, Image-J software, GraphPad Prism 6 SPSS/Windows version 15.0, Frida software (Framework for Image Dataset Analysis), BD FACSuite Software, FLIR-Tools software version 5.11.16337.1002 and AMIDE 0.6 Software. All of this is also mentioned in the Methods section.
Data analysis	Microsoft Excel 2010, Image-J software, GraphPad Prism 6 and SPSS/Windows version 15.0., BD FACSuite Software. All of this is also mentioned in the Methods section.

For manuscripts utilizing custom algorithms or software that are central to the research but not yet described in published literature, software must be made available to editors/reviewers. We strongly encourage code deposition in a community repository (e.g. GitHub). See the Nature Research guidelines for submitting code & software for further information.

Data

Policy information about availability of data

All manuscripts must include a data availability statement. This statement should provide the following information, where applicable:

- Accession codes, unique identifiers, or web links for publicly available datasets
- A list of figures that have associated raw data
- A description of any restrictions on data availability

All data from this manuscript are available form the corresponding author upon request.

Field-specific reporting

Please select the one below that is the best fit for your research. If you are not sure, read the appropriate sections before making your selection.

☒ Life sciences ☐ Behavioural & social sciences ☐ Ecological, evolutionary & environmental sciences

For a reference copy of the document with all sections, see nature.com/documents/nr-reporting-summary-flat.pdf

Life sciences study design

All studies must disclose on these points even when the disclosure is negative.

Sample size	For animal experiments, sample size was chosen based on similar previous studies of our group and on the basis of literature documentation of similar wellcharacterized experiments and statistical methods were not used to predetermine sample sizes. We try to use the fewest number of mice to achieve statistical significance without compromising the outcomes. The sample size are provided in figure legends and in the Statistical. Analysis section in Methods. Sample size on human data was only limited by availability.
Data exclusions	Samples of animals were excluded whether their values were outside the 2SD range. Criteria were pre-established. See Statistics section. For patients, the inclusion and exclusion criteria and treatment protocol are mentioned in the Statistical Analysis section
Replication	All attempts to replicate the experiments have been successful.One way to verify the reproducibility of our experiments findings was that in all the experiments in which we activated the dopamine receptor 2 we have observed a significant decrease in body weight, as well as an increase in the intescapular temperature and the protein levels of UCP1
Randomization	Before start an experiment, all mice groups were made with set of animals of the same sex, age and similar body weight. See Statistical analysis section.
Blinding	For practical reasons, the investigators were not blinded to allocation during experiments and outcome assessment. It is well known that the aim of blinding is to reduce bias due to the knowledge of which intervention is being received by study participants. In many cases, blinding is not possible for example dietary intake in a mice experiment and surgery procedures which are the main experiments in this manuscript. Trying to avoid bias and to achieve treatment balance, the researchers payed big effort randomizing the assignment of each treatment using simple or blocked randomization.

Reporting for specific materials, systems and methods

We require information from authors about some types of materials, experimental systems and methods used in many studies. Here, indicate whether each material, system or method listed is relevant to your study. If you are not sure if a list item applies to your research, read the appropriate section before selecting a response.

Materials & experimental systems

n/a	Involved in the study
☐	☒ Antibodies
☒	☐ Eukaryotic cell lines
☒	☐ Palaeontology
☐	☒ Animals and other organisms
☐	☒ Human research participants
☒	☐ Clinical data

Methods

n/a	Involved in the study
☒	☐ ChIP-seq
☐	☒ Flow cytometry
☒	☐ MRI-based neuroimaging

Antibodies

Antibodies used	The following antibodies were used: UCP1: 1:5000 WB, 1:500 IHQ, ab23841, Abcam, Cambridge, UK Fibroblast Growth Factor-21(FGF21): 1:1000 WB, ab64857, Abcam, Cambridge, UK PRDM16: 1:1000, ab106410 WB, Abcam, Cambridge, UK PGC-1α (H-300): 1:1000, sc-13067 WB, Santa Cruz Biotechnology, CA, USA phospho -SAPK/JNK(Thr183/Tyr185): 1:1000 WB, #4671, Cell Signaling, USA JNK1/3 (C-17): 1:1000, sc-474 WB, Santa Cruz Biotechnology, CA, USA phospho AKT : 1:1000, WB, #9271, Cell Signaling, USA AKT: 1:1000, WB,#9272, Cell Signaling, USA mTOR: 1:1000, WB, SAB4501038, Sigma- Aldrich, St. Louis, MO pro-MCH: 1:1000, WB, sc-28931, Santa Cruz Biotechnology, CA, USA phospho-rpS6: 1:1000 WB, 1:200 IHQ #2211,Cell Signaling, USA Orexin A: 1:1000 WB, bs-15509R,Bioss Antibodies, Massachusetts, USA PDE3B: 1:1000 WB; #PA5-42560, Invitrogen, CA, USA Dopamine D2 Receptor: 1:1000 WB, ab85367, Abcam, Cambridge, UK

S6 ribosomal protein: 1:1000, #2217, Cell Signaling, USA
phospho- CREB (Ser133): 1:1000 WB, #9198, Cell Signaling, USA
Myogenin: 1:1000 WB , F5D, DSHB, Iowa, USA
Myostatin: 1:1000 WB, ab71808, Abcam, Cambridge, UK
α tubulin : 1:5000 WB, T9026, Sigma- Aldrich, St. Louis, MO
β Actin : 1:5000 WB, A5316, Sigma- Aldrich, St. Louis, MO
GAPDH: 1:5000 WB,#CB1001,Merk Millipore, Darmstadt, Germany
c- FOS: 1:500 WB, sc-52, Santa Cruz Biotechnology, CA, USA
GFP: 1:200 IHQ, ab290, Abcam, Cambridge, UK
Chicken anti-GFP: 1:500 IHQ, #A10262,Life Technologies, California, USA
mouse anti-HA:1:1000 IHQ, #MMS-101R, Covance, Princeton, USA
vGlut2: 1:500 IHQ, #135402,Synaptic Systems,Goettingen, Germany
vGat: 1:1000 IHQ, #131013, Synaptic Systems, Goettingen, Germany
Orexin A: 1:500 IHQ, #AB3098, Merk Millipore, Darmstadt, Germany
MCH: 1:500 IHQ, #M8440, Sigma- Aldrich, St. Louis, MO
mCherry: 1:200 IHQ, ab125096, Abcam; Cambridge, UK
The following antibodies were used:
UCP1: 1:5000 WB, 1:500 IHQ, ab23841, Abcam, Cambridge, UK
Fibroblast Growth Factor-21(FGF21): 1:1000 WB, ab64857, Abcam, Cambridge, UK
PRDM16: 1:1000, ab106410 WB, Abcam, Cambridge, UK
PGC-1α (H-300): 1:1000, sc-13067 WB, Santa Cruz Biotechnology, CA, USA
phospho -SAPK/JNK(Thr183/Tyr185): 1:1000 WB, #4671, Cell Signaling, USA
JNK1/3 (C-17): 1:1000, sc-474 WB, Santa Cruz Biotechnology, CA, USA
phospho AKT : 1:1000, WB, #9271, Cell Signaling, USA
AKT: 1:1000, WB,#9272, Cell Signaling, USA
mTOR: 1:1000, WB, SAB4501038, Sigma- Aldrich, St. Louis, MO
pro-MCH: 1:1000, WB, sc-28931, Santa Cruz Biotechnology, CA, USA
phospho-rpS6: 1:1000 WB, 1:200 IHQ #2211,Cell Signaling, USA
Orexin A: 1:1000 WB, bs-15509R,Bioss Antibodies, Massachusetts, USA
PDE3B: 1:1000 WB; #PA5-42560, Invitrogen, CA, USA
Dopamine D2 Receptor: 1:1000 WB, ab85367, Abcam, Cambridge, UK
S6 ribosomal protein: 1:1000, #2217, Cell Signaling, USA
phospho- CREB (Ser133): 1:1000 WB, #9198, Cell Signaling, USA
Myogenin: 1:1000 WB , F5D, DSHB, Iowa, USA
Myostatin: 1:1000 WB, ab71808, Abcam, Cambridge, UK
α tubulin : 1:5000 WB, T9026, Sigma- Aldrich, St. Louis, MO
β Actin : 1:5000 WB, A5316, Sigma- Aldrich, St. Louis, MO
GAPDH: 1:5000 WB,#CB1001,Merk Millipore, Darmstadt, Germany
c- FOS: 1:500 WB, sc-52, Santa Cruz Biotechnology, CA, USA
GFP: 1:200 IHQ, ab290, Abcam, Cambridge, UK
Chicken anti-GFP: 1:500 IHQ, #A10262,Life Technologies, California, USA
mouse anti-HA:1:1000 IHQ, #MMS-101R, Covance, Princeton, USA
vGlut2: 1:500 IHQ, #135402,Synaptic Systems,Goettingen, Germany
vGat: 1:1000 IHQ, #131013, Synaptic Systems, Goettingen, Germany
Orexin A: 1:500 IHQ, #AB3098, Merk Millipore, Darmstadt, Germany
MCH: 1:500 IHQ, #M8440, Sigma- Aldrich, St. Louis, MO
mCherry: 1:200 IHQ, ab125096, Abcam; Cambridge, UK

Validation	All antibodies used in the paper have been validated by the manufacturer and by references . The dilution and the use (Western Blot (WB) or Immunohistochemistry (IHQ) is specified in the previous section. As regards the antibodies used in Western blot in this article, it has been used in both rat and mouse leaving at the appropriate weight in western blot such as shown in the supl fig 11. The specificity of anti-Dopamine D2 receptor, orexin and MCH antibodies were evaluated using WT and KO mice.

Animals and other organisms

Policy information about studies involving animals; ARRIVE guidelines recommended for reporting animal research

Laboratory animals	Male and female Sprague-Dawley rats (standard laboratory diet (CD): 200-250g and high fat diet (HFD) for 12 weeks: 450-700g were used. WT and triple β- adrenoreceptor (AR) knockout (TKO) male mice (weight 20–25 g, age 8–10 weeks old); WT and orexin knockout male mice (null Ox/Hcrt mice (orexin/hypocretin; B6.129S6-Hcrttm1Ywa/J, The Jackson Laboratory) (weight 25–30 g, age 10–12 weeks old), WT and Drd2-cre:ribotag mice (weight 20–25 g, age 8–10 weeks old), vgat-ires-cre knock-in (C57BL/6J) and vglut2-ires-cre knock-in (C57BL/6J) from Jackson Laboratory (weight 20-25g, age 8-10 weeks old) also were used for the experiments. All this information about animal species, sex, strain, provider, etc are mentioned in the Material and Methods section.
Wild animals	This study did not involve wild animals.
Field-collected samples	This study did not involve field collected samples.
Ethics oversight	All experiments and procedures involved in this study were reviewed and approved by the Ethics Committee of the University of Santiago de Compostela, in accordance with European Union normative for the use of experimental animals.

Note that full information on the approval of the study protocol must also be provided in the manuscript.

Human research participants

Policy information about studies involving human research participants

Population characteristics	All patients were of Caucasian origin. Pregnant and lactating women were excluded. Patients with hyperprolactinemia secondary to drugs (including neuroleptics, antidepressants, opiates and gastrointestinal prokinetics) or mixed-secreting tumours or those already receiving dopamine agonists at the first visit to our hospital as well as those not completing a 12-month follow-up period were excluded from the analysis. Patients with multiple pituitary hormone deficiencies and/or the presence of other concomitant causes of overt hypogonadism were excluded to avoid the potential effect of hormonal replacement therapy on body weight control and metabolic changes. In this respect, patients with previously known treatment with hypoglycemic agents to control glucose metabolism abnormalities or anti-obesity drugs for body weight loss were also excluded. After all the exclusions, 31 patients with newly diagnosed prolactinoma comprised the study sample of the retrospective analysis (26 females and 5 males with an age range between 21-61 years). All patients underwent a detailed anamnesis, physical exploration and metabolic evaluation.
Recruitment	All the patients included were affected by hyperprolactinemia and coming from the Endocrinology Department of the University Clinic of Navarra between January 2007 and December 2013. All patients were of Caucasian origin. Pregnant and lactating women were excluded. Patients with hyperprolactinemia secondary to drugs (including neuroleptics, antidepressants, opiates and gastrointestinal prokinetics) or mixed-secreting tumours or those already receiving dopamine agonists at the first visit to our hospital as well as those not completing a 12-month follow-up period were excluded from the analysis. Furthermore, patients with multiple pituitary hormone deficiencies and/or the presence of other concomitant causes of overt hypogonadism were excluded to avoid the potential effect of hormonal replacement therapy on body weight control and metabolic changes. In this respect, patients with previously known treatment with hypoglycemic agents to control glucose metabolism abnormalities or anti-obesity drugs for body weight loss were also excluded
Ethics oversight	Clinical studies were approved, from an ethical and scientific standpoint, by the Hospital's Ethical Committee of the University Clinic of Navarra and were conducted in accordance with the principles of the Declaration of Helsinki with patients giving their informed consent for participation.

Note that full information on the approval of the study protocol must also be provided in the manuscript.

Flow Cytometry

Plots

Confirm that:

☒ The axis labels state the marker and fluorochrome used (e.g. CD4-FITC).

☒ The axis scales are clearly visible. Include numbers along axes only for bottom left plot of group (a 'group' is an analysis of identical markers).

☒ All plots are contour plots with outliers or pseudocolor plots.

☒ A numerical value for number of cells or percentage (with statistics) is provided.

Methodology

Sample preparation	The tuberal region of the hypothalamus of Vgat-cre + Ad-EGFP LHA/ZI mice were microdissected and enzymativcally dissociated using Papain Dissociation System (Worthington, Lakewood, NJ) to obtain single cell suspensions as described previously
Instrument	FACS was performed using an EPICS ALTRA Cell Sorter Cytometer device (BD Bioscience).
Software	BD FACSuite Software
Cell population abundance	The sort decision was based on measurements of EGFP fluorescence (excitation: 488 nm; 50 mW; detection: EGFP bandpass 530/30 nm, autofluorescence bandpass 695/40 nm) by comparing cell suspensions from non-infected brain sites and infected brain sites.
Gating strategy	The sort decision was based on measurements of EGFP fluorescence (excitation: 488 nm; 50 mW; detection: EGFP bandpass 530/30 nm, autofluorescence bandpass 695/40 nm) by comparing cell suspensions from non-infected brain sites and infected brain sites.

☐ Tick this box to confirm that a figure exemplifying the gating strategy is provided in the Supplementary Information.